A NOVEL OPTICAL APPROACH TO THE INTRAOPERATIVE DETECTION OF PARATHYROID GLANDS

By

Constantine A Paras

Dissertation

Submitted to the Faculty of the Graduate

School of Vanderbilt University in partial

fulfillment of the requirements for the

degree of

Doctor of Philosophy

in

Biomedical Engineering

May, 2012

Nashville, Tennessee

Approved:

Professor Anita Mahadevan-Jansen (chair)

Professor Duco Jansen

Professor Robert Galloway

Dr. James Broome

Dr. Edward M. Brown

To Dean

TABLE OF CONTENTS

LIST OF TABLES

LIST OF FIGURES

CHAPTER I

Introduction

Constantine Paras,[1,*]

[1]*Department of Biomedical Engineering, Vanderbilt University, Nashville, TN 37235, USA*

[*]*Corresponding author: anita.mahadevan-jansen@vanderbilt.edu*

Thyroid and parathyroid diseases combine the fields of endocrinology and oncology leading to a complex combination of pathological conditions. When the disease cannot be treated by other methods, surgical means are used to remove the diseased gland(s). Parathyroid glands are difficult to distinguish from the thyroid and surrounding tissues in the neck. The situation is further complicated by its small size and variability in position. Surgeons must ultimately rely on visual inspection to identify the different tissues, which can be subjective and inconclusive. Complications occur when the parathyroid is accidentally injured or removed during thyroidectomies or only partially removed in the case of parathyroidectomies. In the former, hypoparathyroidsim and hypocalcemia can occur resulting in serious side effects. Therefore, there is a need for a sensitive tool that can identify parathyroid glands intraoperatively, regardless of disease state.

Current technology relies on histopathology or post-operative diagnosis of symptoms to determine if the parathyroid was accidentally or incompletely removed. This project is focused on the development of imaging technology specifically, optical imaging and spectroscopy as it pertains to tissue identification. Imaging modalities cover a wide range of topics; within this area, optical techniques deal with the application of light from the ultraviolet to the infrared for identification and visualization of relevant structures. Here, a precursor to optical imaging - optical spectroscopy will be developed for identification and potential imaging of parathyroid tissues for direct clinical application in endocrine surgery. In particular the research and development of near infrared fluorescence spectroscopy and imaging will be presented.

Motivation

This thesis presents a unique application of optical spectroscopy for a critical surgical need in endocrine surgery today. Of the numerous optical techniques, fluorescence spectroscopy is particularly suited for the proposed application. In particular, near-infrared autofluorescence provides a unique avenue for the detection of parathyroid tissues during endocrine surgery regardless of its disease state. It should be noted that biological fluorophores typically exhibit fluorescence in the UV/VIS wavelengths. As excitation wavelengths become longer, autofluorescence decreases. In fact, this reduced fluorescence "background" accounts for the move towards near infrared wavelengths in tissue Raman spectroscopy studies. Thus there are no published accounts of near infrared autofluorescence being observed in tissues.

Near-infrared wavelengths are attractive due to their increased penetration depth in biological tissues. Research in near-infrared fluorescence has mostly involved exogenous contrast agents, the most common of which are polymethines. In particular, indocyanines, such as indocyanine green, and cardio-green has been used extensively as contrast agents for many applications. Inorganic fluorescent semiconductor nanocrystals (quantum dots) solve many instability problems of organic fluorophores and have been used to help identify esophageal sentinel lymph nodes. However, contrast agents are associated with many problems such as potential toxicity, photobleaching and localization. Further, the use of exogenous agents requires additional steps in the safe application of such technology in patients and for future widespread clinical use. Thus, for the speedy implementation of such technology towards a problem that is a practical surgical need today, intrinsic optical spectroscopy is suggested as the most viable candidate for the problem of parathyroid detection. This thesis seeks to develop a method to detect parathyroid tissue through near infrared autofluorescence. This method has the advantages of intrinsic fluorescence and avoids the problems associated with exogenous contrast agents

Specific Aims

The current method for resection of thyroid and parathyroid tissues indicates the need for a diagnostic tool that provides sensitive real-time detection of parathyroid glands during thyroidectomies and parathyroidectomies. The main objective of this project then is to develop a technique based on near- infrared (NIR) autofluorescence that enables intra-operative detection of parathyroid glands such that accidental removal is minimized by supplementing the standards of visual inspection. Since current procedures are guided solely by visual inspection, this thesis presents a novel automated method of surgical guidance that can minimize surgical error and improve patient outcome. The following specific aims are proposed;

Specific Aim (1): Fully characterize the NIR fluorescence signatures of parathyroid and thyroid tissues as well as creating evaluation discrimination algorithms for the detection of parathyroid glands - Fluorescent signatures of thyroid and parathyroid tissues will be characterized in vivo from human patients undergoing thyroidectomies and parathyroidectomies at the Vanderbilt University Medical Center. Fat, muscle and lymph nodes found in the region will also be studied. Tissue will be classified as normal, hyper, hypo or cancerous. Patients will be selected to distribute tissue evenly across all categories. Based on the spectral characteristics of thyroid and parathyroid tissue, discrimination algorithms will be developed using empirical methods. If necessary, multivariate statistical techniques will employed to increase accuracy. The diagnostic algorithms will be implemented on spectra obtained from patients retrospectively. The

capability of NIR fluorescence in predicting the location of the parathyroid glands will be evaluated by comparing it to the sensitivity of visual inspection and using histology when feasible. Thus, a method of validating the ability to provide anatomical guidance regardless of disease state will be identified

Specific Aim (2): Study the basis of observed differences in the spectral characteristics - In developing optical spectroscopy as a tool for endocrinology, the scientific basis for the success of the technique needs to be understood. First, the optical and fluorescence properties of thyroid and parathyroid tissues will be analyzed. Possible candidates with the observed properties will be evaluated by correlating their optical measurements to the spectral characteristics of thyroid and parathyroid tissues. These experiments will provide information to evaluate the biological constituents of the parathyroid and thyroid and identify those that may be responsible for the NIR autofluorescence signal.

Specific Aim (3): Develop a next-generation clinical imaging system - In this section of the project, the goal is to implement new technologies for the hardware of the clinical system. The successful implementation of imaging would provide spatial information increasing utility to the surgeon. This will be accomplished through imaging techniques capable of detecting NIR fluorescence such as a CCD and photo-multiplier tube. If imaging proves unable to provide the same level of sensitivity and accuracy achieved with the fiber-based system, the feasibility of incorporating the fiber system with an endoscope or using a guide-wire will be examined. The

achievement of this goal will simplify the application of fluorescence spectroscopy for tissue differentiation and improve the likelihood of successful translation to the clinic.

The specific aims described above will not only prove the ability of NIR fluorescence to provide consistent and accurate detection, but will also help in developing an understanding of the scientific basis for the success of the technique. The results of this work will have a significant impact on health care by providing guidance towards dissection and resection of thyroid and parathyroid tissues. This would potentially result in fewer complications due to accidental injury or incomplete removal of parathyroid tissue.

CHAPTER II

Background and Significance

Constantine Paras,[1,*]

[1]*Department of Biomedical Engineering, Vanderbilt University, Nashville, TN 37235, USA*

[*]*Corresponding author: anita.mahadevan-jansen@vanderbilt.edu*

Anatomy of the Neck

Endocrine surgery involves exploration of the neck in order to visualize vital tissues for the treatment of benign and malignant conditions of the thyroid and parathyroid glands (1). The general anatomy of this region is illustrated in Figure 1 (2). The thyroid gland is positioned antero-lateral to the larynx and trachea. Generally, there are four parathyroid glands, two superior and two inferior, which tend to lie symmetrically on the posterior surface of the thyroid gland. Important vocal nerves also pass close to the posterior capsule of the thyroid gland including the superior laryngeal and recurrent laryngeal nerves (3, 4). The neck also contains an abundance of lymphatic, vascular, musculoskeletal and adipose tissues as well.

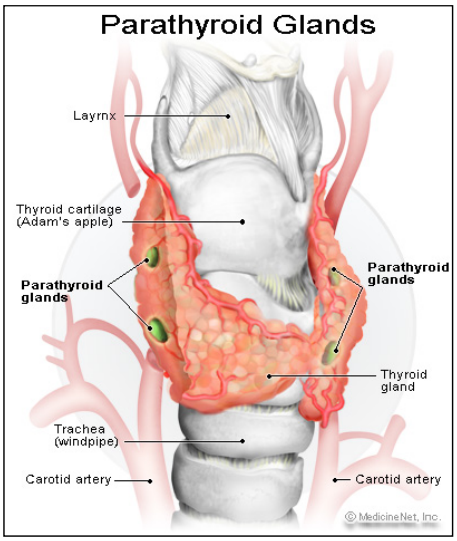

Figure 1: *Anatomy of the central neck (2).*

The parathyroid glands are approximately 6 to 8 mm in size and bean shaped with a yellow-tan to caramel color (size of a grain of rice) (4, 5). The position of the parathyroid glands may vary greatly from patient to patient. The superior and inferior parathyroids make an embryological descent from the 3rd and 4th pharyngeal pouch down to their final resting places behind the thyroid. Aberrant patterns in their migration lead to a large area of the neck and chest in which ectopic parathyroids may be located. Despite this variability, there tends to be symmetry in the positions of the glands on the two sides of the neck. The parathyroid glands are suspended by a small vascular pedicle and

enveloped within a pad of fatty tissue (6). They are comprised of densely packed cells that fall into one of three main types: chief, oxyphil and adipose cells. The glands are primarily composed of chief cells which contain cytoplasmic fat droplets and it is these cells that are primarily responsible for the production of parathyroid hormone (PTH) (7). Parathyroid hormone is an 84-amino acid polypeptide, the secretion of which is responsible for release of calcium and phosphate from bone matrix, calcium reabsorption by the kidney, and regulating renal production of calcitriol, which in turn increases calcium absorption in the intestine. The final effective result of PTH secretion is an increase in plasma calcium concentration (7). Thus, the parathyroid glands maintain the range of calcium concentration in the body important for normal function. While figure 1 clearly indicates the anatomy of the region, it should be noted that conditions are rarely so lucid during endocrine surgeries. The presence of fat, varying locations of the glands and disease state can and *does* often confound the identification the parathyroid.

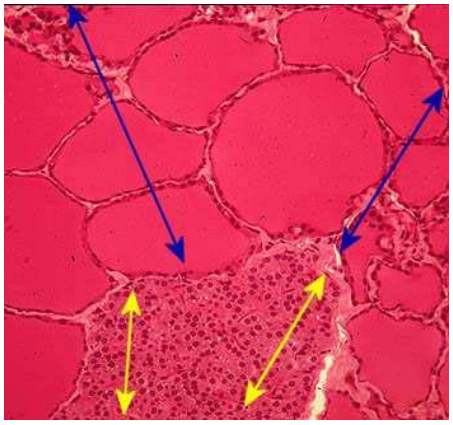

Figure 2: *Thyroid (blue arrows), and parathyroid (yellow arrows) glands under H&E (1).*

The thyroid consists of right and left lobes lying on either side of the trachea joined by the isthmus. Each lobe is about 5 cm long with the total gland weighing 10 to 20 g (3) (8). . Histologically, the functional unit of the thyroid is the follicle. Follicles are a group of epithelial cells spherically arranged around colloid, a solution rich in the protein thyroglobulin (9). Thyroglobulin is a glycoprotein synthesized in the follicular cells and secreted into the colloid. The iodination of tyrosine residues on the thyroglobulin molecule by the enzyme

thyroid peroxidase creates both the T3 and T4 forms of thyroid hormone (8). These two forms of thyroid hormone have diverse and widespread physiologic effects throughout the human body (9). Histology can be used to identify the various normal tissues discussed previously. Figure 2 is a histological section showing the transition between thyroid and parathyroid tissue. The blue arrows in the figure highlight the thyroid tissue where follicles surrounding large collections of colloids are evident. Yellow arrows mark parathyroid tissue containing the chief and oxyphil cells.

Diseases in the neck

Primary *hyperparathyroidism* (HPT) is a relatively common condition with annual incidence rates of 25-28 cases per 100,000 people (10, 11). The rate is higher in Caucasian women above 60 years old, approaching 190 cases per 100,000 annually (11). Typically, HPT is characterized by excessive secretion of PTH, which in turn results in elevated levels of plasma calcium. In approximately 80% of cases, primary HPT is caused by a benign tumor designated as *parathyroid adenoma* (12). In about 15% of these cases, more than one gland is involved making accurate identification of the parathyroids of paramount importance. Surgical excision of abnormal glands is advocated for young (<50 years of age) or symptomatic patients with primary HPT. Symptoms vary widely and include such complaints as muscle weakness, bone pain, nephrolithiasis, fatigue, constipation, peptic ulcers, and severe osteoporosis (13). The thyroid gland, parathyroid glands, nerves, adipose tissue, and lymph nodes are closely positioned in the central neck (Level VI). Due to their close proximity and tendency to blend into one

another, many of these structures, specifically the parathyroid glands, are difficult to distinguish visually during endocrine surgery.

Functional thyroid disease occurs when the thyroid gland does not supply the appropriate amount of thyroid hormone needed. Currently, about 20 million Americans have some form of thyroid disease. People of all ages and races can get thyroid disease; however, women are five to eight times more likely than men to have thyroid problems (14). If the thyroid is overactive, it releases too much thyroid hormone into the bloodstream, resulting in **hyperthyroidism**. An underactive thyroid produces too little thyroid hormone, resulting in **hypothyroidism.** Both conditions can result in the thyroid becoming larger than normal. When it is large enough to see easily, it's called a **goiter**. *Graves disease*, an autoimmune disorder, is the most common cause of hyperthyroidism wherein increased abnormal antibodies result increased production of thyroid hormone. Eventually, the thyroid gland enlarges, which can result in a goiter. When the condition cannot be controlled with medication, surgery is often performed to remove the diseased thyroid gland.

Thyroid nodules can sometimes occur in a normal working thyroid. With physican awareness and the use of ultrasound, up to 20% of the population may be diagnosed with a thyroid nodule (14). While most nodules are benign, approximately 5 to 15% may harbor some form of thyroid cancer (14). Approximately 37,200 new cases of thyroid cancer will be diagnosed in the United States in 2009. The disease is most common in young people, with nearly two-thirds of diagnosed cases in people between the ages of 20 and 55. Since 1997, there has been a 6% yearly increase in the likelihood of being diagnosed with thyroid cancer. This may be due to the increasing use of ultrasound to

detect small thyroid nodules. The main treatment of thyroid cancer is a thyroidectomy, or surgical removal of all or part of the affected thyroid gland (15). Thyroid surgery is considered one of the safest surgical procedures; however, it necessitates careful dissection of the thyroid avoiding injuring vital structures such as the parathyroids (16).

There are several possible complications related to thyroid surgery such as hypocalcemia and hypoparathyroidism (5). Within 2 to 5 days after total or subtotal thyroidectomy, a decrease of serum calcium, a condition known as hypocalcemia, is frequently observed. The incidence of hypocalcemia is reported to occur in 1.6% to more than 50% of thyroidectomies. The most probable cause is hypoparathyroidism due to trauma, devascularization, or inadvertent removal of one or more parathyroid gland(s) during surgery (17). This condition is categorized as either transient or permanent. In the case of transient hypocalcemia, within a few weeks to months serum calcium levels normalize as function of the parathyroid is recovered. Permanent hypocalcemia lasts more than 6 months and is associated with significant impairment of quality of life. Chronic gastrointestinal discomfort, painful myalgias, parathesias, changes in bone metabolism and development of cataracts are a few of the possible resulting symptoms (18). A patient with permanent hypoparathyroidism requires large amounts of calcium and vitamin D supplements for the remainder of their life often necessitating 12 to 15 pills evey day to maintain physiologic calcium levels [4]. This represents a significant source of morbidity to the patient (5). Hypocalcemia is the most common cause of malpractice litigation after endocrine surgery (17). Accordingly, effective management of thyroid diseases is dependent on parathyroid preservation during thyroidectomy (5). In the literature, the incidence of inadvertent parathyroidectomy ranges from 8% to 19% of

patients undergoing total thyroidectomy (19). Complication rates have been shown to be directly proportional to the extent of the thyroidectomy, and inversely proportional to operating surgeon's experience level. The rate is also related to the extent of the invasion of the thyroid cancer. Consequently, the surgeon's familiarity of the parathyroid glands' anatomy and blood supply is imperative to safe tissue removal (5).

Current localization techniques

Existing methods for identifying parathyroid glands are limited in their applicability and sensitivity and are, thus, not adequate enough to prevent surgical complications (20). Primary means include ultrasound, sestamibi scintigraphy, CT, MRI and intraoperative intact Parathyroid Hormone (iPTH) assay. Ultrasound is one of the most common techniques for imaging the neck and has sensitivity ranging from 27 – 85% (13, 21). The normal parathyroid gland is not typically visualized because of its deep location and small size; ultrasound is mainly used to locate parathyroid adenomas larger than 1 cm. It has the advantages of being fast cheap and relatively harmless but yields suboptimal results patients with a short thick neck requiring a lower frequency transducer which decreases spatial resolution and adenomas located in "silent," low contrast, US areas of the neck (13, 21). Thyroid complications often occur simultaneously with parathyroid disease which further restricts the use of US because in patients with multi-nodular thyroid disease, nodules can mimic or mask adenomas. Lymph nodes can also easily be mistaken for adenomas.

Nuclear imaging is based on the different radiotracer uptake patterns and kinetics between the thyroid gland, normal parathyroid and abnormal parathyroid. Specifically, radioiodine is taken up and organified by the thyroid (which uptakes iodine normally) whereas blood flow tracers such as ^{201}thallous chloride and ^{99m}Tc sestamibi are used to identify both the thyroid and enlarged parathyroid glands. The most common use is the injection of Technetium ^{99m}Tc labelled 2 –methoxy-isovutyl-isonitrile (sestamibi) and is often considered the gold standard for pre-operative localization of hyperfunctioning parathyroid tissue. Overactive parathyroid glands tend to absorb the tracer more than the surrounding tissue. Patients are imaged using single photon emission computed tomography (SPECT) after the tracer is administered. Sestamibi scintigraphy can detect abnormally located parathyroid adenomas with more than 90% accuracy but requires administration of a radiopharmaceutical, use of sophisticated scanning equipment and well-trained operators. Due to the small size of the parathyroid gland the sestamibi scan can give false-negatives or recognize some thyroid diseases as a false-positive due to uptake of the tracer (13, 21). As a result, a second image is usually taken hours after the initial image because adenomas should display delayed washout of the tracer due to their hyperactivity.

In order to overcome the limitations with sensitivity of imaging techniques, some physicians have tried supplementing preoperative imaging with CT and MRI. Thin-section, contrast-enhanced CT has been used with reported sensitivity ranging from 46 – 87%. CT is most often used in addition to ultrasound in order to find abnormal glands in nonresponsive areas. It is also used to agree with sestamibi findings. CT is better at detecting harder to find parathyroid adenomas over ultrasound but is susceptible to

movement artifacts during imaging and exposes the patient to ionizing radiation. As in ultrasound, lymph nodes can also be mistaken for adenomas. (13, 21). Similarly, MRI has been used in recent years with a sensitivity of 65 – 80%. MR is another option that is used to confirm results rather than a first line technique. Adenomas can appear much more intense in T2-weighted images but only 40% of masses exhibit this effect. Due to limited availability, high cost and long examination time, MRI is still not widely used (13).

Current intraoperative techniques include iPTH and radio-guided parathyroidectomy. Intra-operative assays are a measure of the levels of parathyroid hormone in the blood. Once the hyperfunctioning gland is removed, the amount of PTH will gradually return to normal. However, PTH starts to degrade around four minutes so the samples must be rushed to the testing lab which is located outside the OR. Additionally, the assays are expensive and are only available at centers that perform a high volume of parathyroidectomies (10). Radio-guided parathyroidectomy involves the intravenous administration of technetium-99m-sestamibi 1-2 hours before surgery. A hand-held gamma probe is used to localize the abnormal glands, however, the radiation background is unvalidated and the technique is susceptible to non-selective uptake of the radionucleotide as in the preoperative method (10, 13). There is the need to guide surgery in real-time with high accuracy.

Optical Spectroscopy

Optical spectroscopy has been studied for many years as a non-intrusive, real-time automated tool for tissue detection. However, these studies have typically been pursued for detection of pathology. In this proposal, I suggest the application of optical spectroscopy for the physiological detection of the parathyroid because it can detect differences in tissue architecture and biochemical composition. One such optical technique studied extensively for optical diagnosis in recent years is Raman spectroscopy, a technique that has been used for many years to probe into the biochemistry of various biological molecules (22, 23). Raman scattering is an inelastic scattering process, which arises from perturbations of the molecule that induces vibrational or rotational transitions (24). Thus Raman spectroscopy is a molecular specific technique that can be used as a biochemical tool for the study of different materials; in particular this technique has the capability to provide differential diagnosis of pre-cancers and cancers. While many challenges prevented the widespread application of Raman spectroscopy for disease detection, recent developments in detector and source technologies have resulted an increased number of reports published on the application of Raman spectroscopy for the detection of cancers *in vivo,* in organs such as the cervix, skin, breast and the gastrointestinal tract (GI) (25-29) with high sensitivities and specificities. Raman spectroscopy is extremely sensitive to subtle changes in tissue physiology as well as pathology. However, it is a weak phenomenon and in vivo imaging with Raman spectroscopy is not yet feasible. Other optical techniques applied to medical diagnosis include diffuse reflectance/elastic scattering spectroscopy, optical coherence tomography, and infrared spectroscopy to name a few.

Application of optical spectroscopy to endocrine surgery is currently limited. Several groups have applied autofluorescence spectroscopy with excitation in the ultraviolet and visible wavelengths as well as Raman spectroscopy for the discrimination of laryngeal and thyroid cancers from normal tissues (30-36). One group demonstrated the use of 5-aminolevulimic acid (ALA) to guide parathyroidectomies due to secondary hyperparathyroidism. Increased ALA fluorescence with HPT resulted in strong fluorescence contrast of (hyper) parathyroid tissue compared to background soft tissues and thyroid thereby demonstrating the potential of using 5-ALA to guide dissection in parathyroidectomies [36]. Early work was performed in rats and the most recent publication (in 2006) presented the application of this technique in 1 patient [ref n]. No further publications were found by this group. Das et al. used NIR Raman spectroscopy for *ex-vivo* diagnosis of adenoma and hyperplasia in parathyroid tissue in patients undergoing parathyroidectomies. The results showed a detection sensitivity of 95% for parathyroid adenomas and 93% for hyperplasia [35]. However, all of these studies are focused on disease detection. No papers were found that applied optical methods for the identification of normal parathyroid compared to all other tissues.

Of the many optical techniques, fluorescence spectroscopy has been of considerable interest in the development of new clinical diagnostic tools. Fluorescence measurements of human tissue can be made in real-time, without tissue removal and diagnosis based on tissue fluorescence can be easily automated (37). Fluorescence spectroscopy is the most commonly tested optical technique for the *in vivo* detection of diseases. Further, fluorescence imaging is feasible and can reveal the localization and measurements of intracellular molecules, sometimes at the level of single-molecule detection.

Fluorescence is now a dominant methodology used extensively in biotechnology, flow cytometry, medical diagnostics, DNA sequencing and forensics to name just a few. Fluorescence spectroscopy of both exogenous and endogenous fluorophores has been successfully used to identify neoplastic cells and tissues in a variety of organ systems (38). Studies have successfully demonstrated the potential of fluorescence to improve diagnosis in various organ systems [42-50]. Intrinsic tissue fluorescence (autofluorescence) has been used to differentiate normal and non-normal tissues in the human breast and lung [44], brain [43], oral mucosa [47], cervix [46].

Fluorescence Spectroscopy

The unique electron structure associated with a molecule exist in distinct energy states which they can occupy known as singlet states. Electrons normally occupy the ground state, S_o, which requires the least energy. Within each singlet state the electron can have slightly different energy corresponding to different vibrational frequencies. When light interacts with tissue it can be reflected, scattered or absorbed. The amount of energy absorbed is dictated by the singlet states of the electrons. When incident photons contain energy equal to gap between singlet states, electrons will absorb enough energy to jump up to one of the higher states. The electron

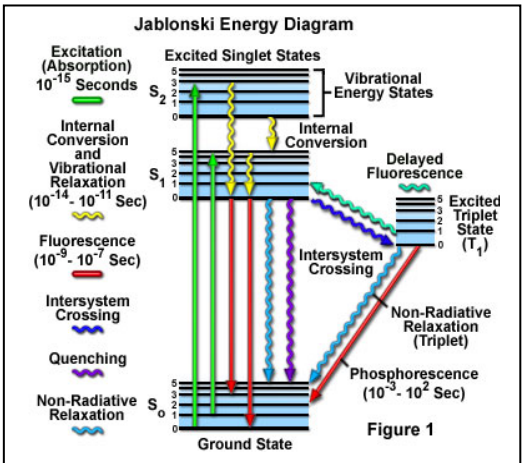

Figure 3: *Jablonski diagram illustrating the various processes including fluorescence (40).*

does not remain excited and will eventually drop back down to the ground state. With a few rare exceptions, molecules in condensed phases rapidly relax to the lowest vibrational level of S_1 (39). So, if it is excited to a higher state, it will first lose energy due to heat and vibrational movement to drop, this is known as internal conversion. Once it returns to the ground state it releases energy in the form of a photon. Due to energy lost from heat and vibration the photon is released at a longer wavelength than was absorbed. This phenomenon is illustrated in figure 3 which is known as a Jablonski diagram (39). One of the important factors is the energy of the excitation light. Electrons are more likely to absorb a photon if the energy is approximately the difference between the different singlet states. So, there is an optimal wavelength for each material that will induce the maximum fluorescence in a given region of the electromagnetic spectrum.

Due to the discrete levels of energy each molecule has a characteristic emission spectrum which is generally the mirror image of the absorption spectrum. The symmetry is the result of the same energy transitions being involved in both absorption and emission. The loss of energy between absorption and emission causes the emitted photon to have a lower frequency and longer wavelength. This shift is known as the Stokes Shift. An important property of fluorescence is that the same emission spectrum is observed in regards to wavelength of light despite the excitation wavelength used. So, based on the

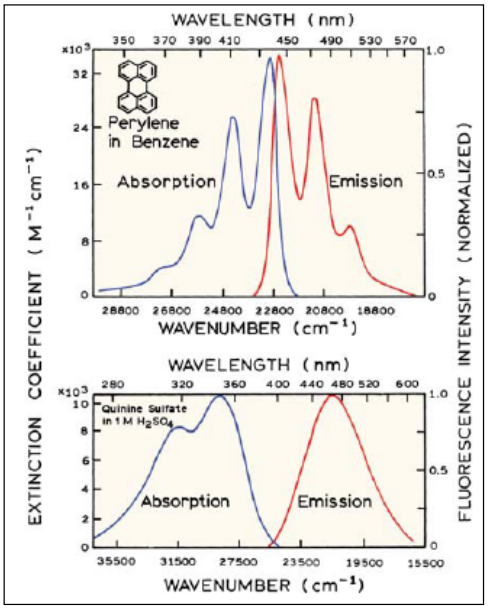

Figure 4: *Typical absorption and emission spectra (40).*

molecules that fluoresce in a given compound, each compound has characteristic excitation emission wavelength(s) at which peak fluorescence occurs (39). Examples of typical absorption and emission spectra are presented in figure 4.

The actual molecule that fluoresces is known as the fluorophore. Fluorophores are classified as either intrinsic or extrinsic. Intrinsic fluorophores occur naturally while extrinsic fluorophores are added in order to induce fluorescence. For example, cell membranes and DNA do not typically fluoresce strongly, therefore an extrinsic fluorophore in the form of a specific molecule or dye that will bind to the target is added. Extrinsic fluorophores typically have stronger fluorescence than intrinsic and are used to produce contrast. Intrinsic fluorophores are typically aromatic compounds containing one or more benzene rings. Aromatic compounds have an excess of conjugated bonds forming an electron cloud resulting in delocalized electrons that are free to absorb light and produce fluorescence.

The majority of research in near-infrared fluorescence has mostly involved exogenous contrast agents, the most common of which are polymethines. In particular, indocyanines, such as indocyanine green, and cardio-green has been used extensively as contrast agents for many applications. Inorganic fluorescent semiconductor nanocrystals (quantum dots) solve many instability problems of organic fluorophores and have been used to help identify esophageal sentinel lymph nodes [37, 38]. However, contrast agents are associated with many problems such as potential toxicity, photobleaching and localization. Further, the use of exogenous agents requires additional steps in the safe application of such technology in patients and for future widespread clinical use. Thus, for the speedy implementation of such technology towards a problem that is a practical

surgical need today, intrinsic optical spectroscopy is suggested as the most viable candidate for the problem of parathyroid detection. This method has the advantages of intrinsic fluorescence and avoids the problems associated with exogenous contrast agents.

Biological fluorophores mostly emit light between the UV and visible portions of the spectrum or about 400-700 nm (39). As excitation wavelengths become longer, autofluorescence decreases (40).. In fact, this reduced fluorescence "background" accounts for the move towards near infrared wavelengths in tissue Raman spectroscopy studies. Thus there are no published accounts of near infrared autofluorescence being observed in tissues. However, near-infrared wavelengths are attractive due to their increased penetration depth in biological tissues. There have been recent efforts to use NIR wavelengths for fluorescence spectroscopy in the diagnosis and detection of disease. One group took advantage of NIR autofluorescence in conjunction with cross-polarized light scattered images to detect breast cancer, but this work was on the edge of the NIR window using 632.8 nm excitation (41). Another group used NIR autofluorescence to detect melanin distribution in the skin (42).

An accurate, automated diagnostic method could allow faster, more effective patient management. The application of optical spectroscopy is suggested because it can detect differences in tissue architecture and biochemical composition. Fluorescence measurements of human tissue can be made in real-time, without tissue removal and diagnosis based on tissue fluorescence can be easily automated. Fluorescence spectroscopy is the most commonly tested optical technique for the *in vivo* detection of diseases. Fluorescence imaging can reveal the localization and measurements of intracellular molecules, sometimes at the level of single-molecule detection. Thus this

proposal presents a unique application of optical spectroscopy for a critical surgical need in endocrine surgery today. Of the numerous optical techniques, we propose to use fluorescence spectroscopy for this purpose. In particular, we propose to use near-infrared autofluorescence for the detection of parathyroid tissues during endocrine surgery, regardless of disease state.

Previous Research

Preliminary to the proposed research, a set of feasibility studies were performed to evaluate the potential application of optical spectroscopy for discrimination between thyroid and parathyroid tissues. Fluorescence, diffuse reflectance and Raman spectra were acquired from thyroid, parathyroid and other normal tissues found in the neck region. Results from the Raman analysis as well as early fluorescence analysis show that parathyroid tissues have a distinct signature compared to all other tissues in the near infrared that can be used to differentiate parathyroid tissues automatically in real time. The results of these studies are discussed below.

In vitro studies

The feasibility of differentiating various endocrine tissues, particularly the parathyroid, was first evaluated using a fiber optic based combined fluorescence and diffuse reflectance system that excites fluorescence at 337 nm and acquires diffuse reflectance between 400-800 nm. However, spectra acquired from canine as well as

human tissues showed no significant consistent differences between the various tissue types (Figure 5). Raman spectroscopy is sensitive to biochemical differences between tissues, so the application of Raman spectroscopy was evaluated in an *in vitro* study. Swine and canine fat, lymph node, thyroid, and parathyroid samples were obtained to evaluate spectral signatures of each sample type. Like humans, canines have four parathyroid glands located in the neck. Grossly, the parathyroid glands of canines appear similar to humans, having the same fleshy color and ranging from 2-6 mm in size [16]. Histologically, both canine and human parathyroid glands are made of chief and oxyphil cells as well as fibrovascular stroma and adipose tissue. The parathyroid glands of canines function similar to their human counterparts, serving to regulate the body's calcium levels. Like humans, canine parathyroid glands modulate levels of calcium based on a delicate balance between PTH, calcitonin and Vitamin D [15]. In addition, canine parathyroid glands are subject to the same disease processes as humans, including hyperplasia and adenomas [17, 18].

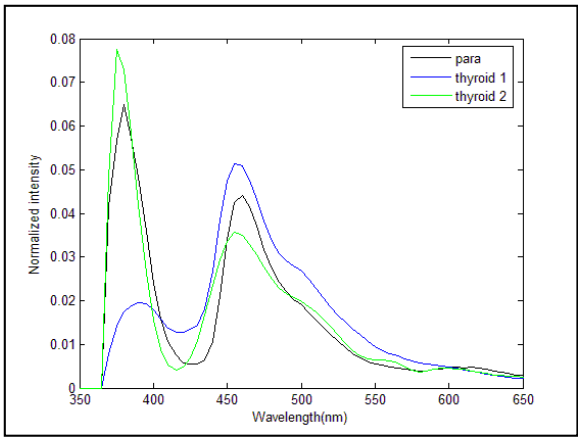

Figure 5: *Fluorescence spectra of parathyroid and thyroid tissues at 337 nm excitation.*

A portable Raman spectroscopy system, shown in Figure 6**,** assembled at the Vanderbilt University Biomedical Optics Laboratory was used to acquire the Raman spectra**.** The system consists of a 785 nm diode laser (Innovative Photonic Solutions, NJ), a fiber optic probe (EMVision, FL), imaging spectrograph (Kaiser Optical Systems, Inc., MI), and back-illuminated, deep-depletion, charge coupled device (CCD) camera

(Andor Technology, CT), all controlled with a laptop computer. The fiber optic probe delivered 80 mW of the incident light to the tissue and collected the scattered light for up to 3 s. The fiber optic probe was maintained in contact with the tissue during each measurement with the overhead fluorescent lights turned off.

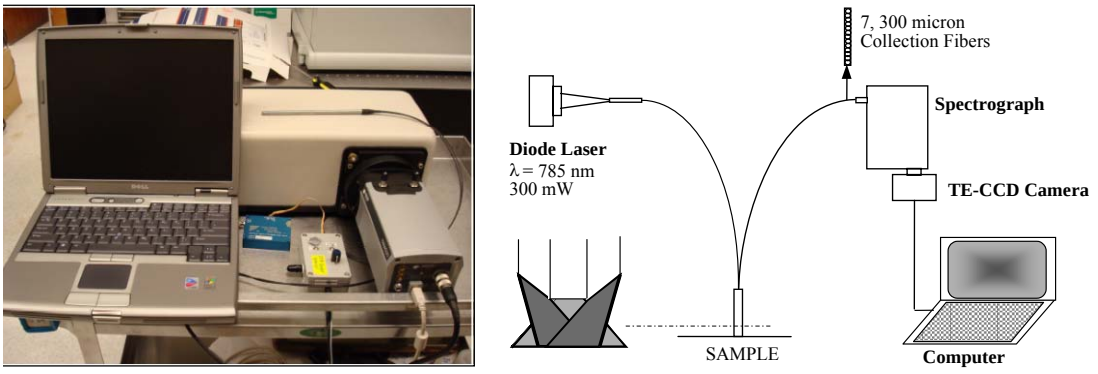

(a) (b)

Figure 6: *(a) Image of the clinical Raman system, (b) Schematic of the Raman system.*

The most striking characteristic seen in these measurements was the saturation of the raw signal acquired from the parathyroid tissue of both animal models. The integration time was reduced from 3 s to 30 ms before a non-saturated signal could be acquired and processed for Raman signal extraction. Conversely, the raw Raman spectra of the other tissue types did not saturate with an integration time of 3s. Additionally, the subcutaneous adipose tissue spectra contained distinct Raman peaks characteristic of fat. To evaluate if the signal saturation observed in parathyroid tissue was distinct to animal tissues, *in vitro* human tissue samples were then measured. The same Raman system was used as before. Spectra were collected in the same manner with the lights off. Similar saturation from parathyroid tissues was observed down till 30 ms before Raman signal could be acquired; similar to spectra from swine and canine samples.

In vivo Raman study

The initial *in vitro* studies demonstrated that a distinctly strong signal was acquired at 785 nm excitation from parathyroid tissue, animal and human compared to all other tissues. However, such signal behavior had not been previously observed and thus the validity of the observation was questioned. Since our lab has successfully applied Raman spectroscopy *in vivo*, a pilot study was designed to verify the presence of the strong parathyroid signal in patients undergoing surgery. This would allow for the realization of the full potential of optical spectroscopy to provide real-time, automated information of parathyroid and surrounding tissue for identification intraoperatively.

Thus, Raman spectra of parathyroid, thyroid, neck lymph nodes, nerve and subcutaneous fat in 26 patients were collected. These spectra were obtained using the same Raman system shown in Figure 4. The probe was sterilized between each case. Patient consent was received from each patient following the approval of the protocol by the Vanderbilt University Institutional Review Board (IRB). Dr. John Phay, an assistant professor of the Department of Surgical Oncology at VUMC, recruited the patients. Each patient's final eligibility for participating in the study was determined during preoperative evaluation deeming the individual as a safe and acceptable candidate. Only adult patients between the ages of 18-99 years with primary thyroid or parathyroid pathophysiology undergoing thyroidectomy or parathyroidectomy were considered.

Following exposure of the relevant region of the neck, the sterilized optical probe was placed on various tissues and Raman spectra were acquired from each of those sites. The tissue type was noted, and the physician's confidence in visual identification was

recorded. Spectra were collected using a 3 s signal collection time. If the signal saturated, the fiber optic probe was kept in contact with the tissue and the signal collection time was reduced to 1 s. If saturation was observed at 1 s, the signal collection time was again reduced to 0.1 s. In all cases, the overhead fluorescent lights were turned off during the measurements. Any luminescent lights left on were turned away from the measurement site. When the tissue was removed in the course of the surgery, histological identification of the specimens from which measurements were taken was obtained following routine surgical histopathology.

Figure 7 demonstrates a sample series of spectra acquired from a typical patient. As can be clearly seen, parathyroid tissue continued to demonstrate raw signal saturation at 3 s. The relative signal strength acquired at 3 s integration compared to 1 s can also be observed. Such results were consistently observed in most patients in this study. These results clearly indicated that there was a stronger intrinsic fluorescence/luminescence signal that was observed in the parathyroid tissue as compared to thyroid as well as other tissues at 785 nm. The level of fluorescence observed in the fat and neural tissues was found to be typical to that observed in other tissue studies such as the skin and the cervix. Processed Raman spectra were difficult to

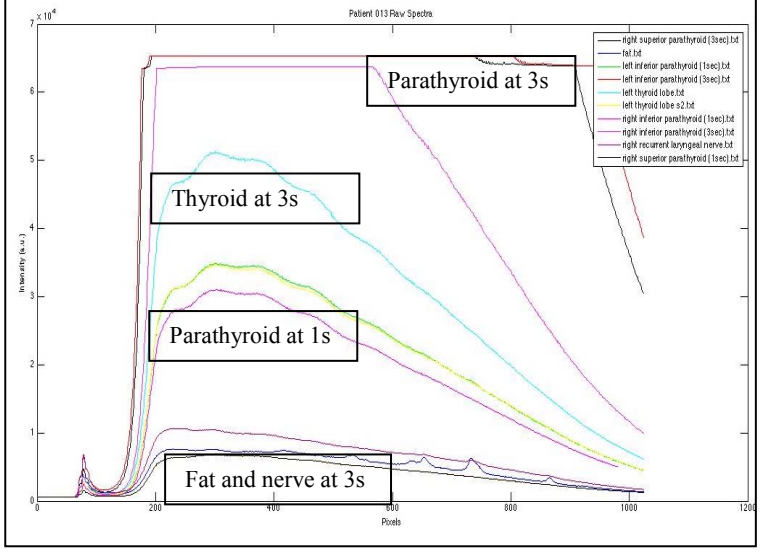

Figure 7: *Raman spectra of a typical patient.*

evaluate due to the poor signal to noise of the parathyroid spectra (acquired at 0.1 s integration).

Summary

This initial study aimed to investigate if parathyroid tissue had unique optical signals that could be used to identify the parathyroid glands and differentiate them from other tissues in the neck intra-operatively. These results clearly indicated (a) the feasibility of acquiring optical signals from various tissues in a clinically feasible time, and (b) the strong signal from parathyroid tissues that allows its identification. This study showed the potential for optical spectroscopy, specifically Raman, to differentiate parathyroid glands from the surrounding tissues in the neck region. However, this study also negated the need for Raman spectroscopy for the identification of the parathyroid. Since the most significant differences were observed in the broadband signal acquired at 785 nm, it was hypothesized that sensitive Raman instrumentation was not necessary for this study. Instead, a simple NIR fluorescence instrument would suffice for the goal of this project – parathyroid identification. In order to test this hypothesis, another pilot study was conducted to assess the feasibility of intrinsic NIR fluorescence at 785 nm excitation to identify parathyroid tissue intra-operatively.

References

1. J. Hubbard, W. B. Inabnet, C-Y. Lo, "Endcrine Surgery" (1st Edition), Springer, (2011).

2. Medicinenet, "Parathyroid Glands," p. Anatomy of neck region, http://www.medicinenet.com/parathyroidectomy/article.htm (2007)
3. R. D. Bliss, P. G. Gauger and L. W. Delbridge, "Surgeon's approach to the thyroid gland: surgical anatomy and the importance of technique," World J Surg 24(8), 891-897 (2000)
4. F. R. Miller, "Surgical anatomy of the thyroid and parathyroid glands," Otolaryngol Clin North Am 36(1), 1-7, vii (2003)
5. A. R. Shaha and B. M. Jaffe, "Parathyroid preservation during thyroid surgery," American journal of otolaryngology 19(2), 113-117 (1998)
6. H. N. Le and J. A. Norton, "Parathyroid," in Essential Practice of Surgery (J. A. Norton, R. R. Bollinger, A. E. Chang, S .F. Lowery, S. J. Mulvihill, H. I. Pass, R. W. Thompson – Editors), pp. 369-378, Springer (1st Edition), (2003).
7. A. H. Elgazzar, "Parathyroid Gland," in The Pathophysiologic Basis of Nuclear Medicine, (A. H. Elgazzar – Editor), pp. 222-237, Springer (2nd Edition), (2006).
8. I. R. McDougall, "Management of thyroid cancer and related nodular disease", Springer,)1st Edition), (2006).
9. S. Nussey, S. Whitehead, " Endocrinology", BIOS Scientific Publishers, (2001).
10. L. Kim, M. W. Krause, V. Kantorvich, "Hyperparathyroidism," (G. T. Griffing – Editor), http://emedicine.medscape.com/article/127351-overview , (2011).
11. J. A. Sosa, N. R. Powe, M. A. Levine, R. Udelsman and M. A. Zeiger, "Profile of a clinical practice: Thresholds for surgery and surgical outcomes for patients with primary hyperparathyroidism: a national survey of endocrine surgeons," J Clin Endocrinol Metab 83(8), 2658-2665 (1998)

12. D. Scott-Coombes, "The parathyroid glands: hyperparathyroidism and hypercalcaemia," Surgery (Oxford) 21(12), 309-312 (2003)

13. A. T. Ahuja, K. T. Wong, A. S. Ching, M. K. Fung, J. Y. Lau, E. H. Yuen and A. D. King, "Imaging for primary hyperparathyroidism--what beginners should know," Clin Radiol 59(11), 967-976 (2004)

14. ATA, "Thyroid Surgery," American Thyroid Association, http://www.thyroid.org/patients/brochures/ThyroidSurgery.pdf, (2005).

15. ACS, "Detailed Guide: Thyroid Cancer," American Cancer Society, http://www.cancer.org/Cancer/ThyroidCancer/DetailedGuide/index, (2008).

16. D. T. Lin, S. G. Patel, A. R. Shaha, B. Singh and J. P. Shah, "Incidence of inadvertent parathyroid removal during thyroidectomy," The Laryngoscope 112(4), 608-611 (2002)

17. F. Pattou, F. Combemale, S. Fabre, B. Carnaille, M. Decoulx, J. L. Wemeau, A. Racadot and C. Proye, "Hypocalcemia following thyroid surgery: incidence and prediction of outcome," World J Surg 22(7), 718-724 (1998)

18. A. Frilling and F. Weber, "Complications in Thyroid and Parathyroid Surgery," in Surgery of the Thyroid and Parathyroid Glands (D. Oertili, R. Udelsman – Editors), pp. 217-224, (1st Edition), (2007).

19. G. H. Sakorafas, V. Stafyla, C. Bramis, N. Kotsifopoulos, T. Kolettis and G. Kassaras, "Incidental parathyroidectomy during thyroid surgery: an underappreciated complication of thyroidectomy," World J Surg 29(12), 1539-1543 (2005)

20. R. L. Prosst, J. Gahlen, P. Schnuelle, S. Post and F. Willeke, "Fluorescence-guided minimally invasive parathyroidectomy: a novel surgical therapy for secondary hyperparathyroidism," Am J Kidney Dis 48(2), 327-331 (2006)

21. S. Fakhran, B. F. t. Branstetter and D. A. Pryma, "Parathyroid imaging," Neuroimaging Clin N Am 18(3), 537-549, ix (2008)

22. A. Mahadevan-Jansen and R. Richards-Kortum, "Raman Spectroscopy for the detection of cancers and precancers," J Biomed Opt 1(1), 31-70 (1996)

23. E. B. Hanlon, R. Manoharan, T. W. Koo, K. E. Shafer, J. T. Motz, M. Fitzmaurice, J. R. Kramer, I. Itzkan, R. R. Dasari and M. S. Feld, "Prospects for in vivo Raman spectroscopy," Physics in medicine and biology 45(2), R1-R59 (2000)

24. R. J. Colthrup, L. H. Daly, S. E. Wiberley Infrared and Raman spectroscopy, Academic Press (3rd Edition), (1991).

25. M. V. P. Chowdary, K. K. Kumar, J. Kurien, S. Mathew and C. M. Krishna, "Discrimination of normal, benign, and malignant breast tissues by Raman spectroscopy," Biopolymers 83(5), 556-569 (2006)

26. T. R. Hata, T. A. Scholz, I. V. Ermakov, R. W. McClane, F. Khachik, W. Gellermann and L. K. Pershing, "Non-invasive Raman spectroscopic detection of carotenoids in human skin," Journal of Investigative Dermatology 115(3), 441-448 (2000)

27. M. G. Shim, L. Song, N. E. Marcon and B. C. Wilson, "In vivo near-infrared Raman spectroscopy: Demonstration of feasibility during clinical gastrointestinal endoscopy," Photochemistry and Photobiology 72(1), 146-150 (2000)

28. A. P. Oliveira, R. A. Bitar, L. Silveira, R. A. Zangaro and A. A. Martin, "Near-infrared Raman spectroscopy for oral carcinoma diagnosis," Photomedicine and Laser Surgery 24(3), 348-353 (2006)

29. A. Mahadevan-Jansen, W. F. Mitchell, N. Ramanujam, U. Utzinger and R. Richards-Kortum, "Development of a fiber optic probe to measure NIR Raman spectra of cervical tissue in vivo," Photochemistry and Photobiology 68(3), 427-431 (1998)

30. C. Arens, K. Malzahn, O. Dias, M. Andrea and H. Glanz, "[Endoscopic imaging techniques in the diagnosis of laryngeal carcinoma and its precursor lesions]," Laryngo- rhino- otologie 78(12), 685-691 (1999)

31. G. Giubileo, F. Colao, A. Puiu, G. Panzironi, F. Brizzi and P. Rocchini, "Fluorescence spectroscopy of normal and follicular cancer samples from human thyroid," Spectroscopy 19(2), 79-87 (2005)

32. G. Liu, J. H. Liu, L. Zhang, F. Yu and S. Z. Sun, "Raman spectroscopic study of human tissues," Guang Pu Xue Yu Guang Pu Fen Xi (Chinese Journal – Translated to English), 25(5), 723-725 (2005)

33. C. Medina-Gutierrez, J. L. Quintanar, C. Frausto-Reyes and R. Sato-Berru, "The application of NIR Raman spectroscopy in the assessment of serum thyroid-stimulating hormone in rats," Spectrochim Acta A Mol Biomol Spectrosc 61(1-2), 87-91 (2005)

34. M. J. Pitman, J. M. Rosenthal, H. E. Savage, G. Yu, S. A. McCormick, A. Katz, R. R. Alfano and S. P. Schantz, "The fluorescence of thyroid tissue," Otolaryngol Head Neck Surg 131(5), 623-627 (2004)

35. R. L. Prosst, F. Willeke, L. Schroeter, S. Post and J. Gahlen, "Fluorescence-guided minimally invasive parathyroidectomy: a novel detection technique for parathyroid glands," Surg Endosc 20(9), 1488-1492 (2006)

36. Z.V. Jaliashvili, T.D. Medoidze, K.M. Mardaleishvili, J.J. Ramsden, Z.G. Melikishvili "Laser induced fluorescence model of human goiter," Laser Meth Chem Biol Med, 5(3) pp. 217-219 (2008).

37. N. Ramanujam, M. F. Mitchell, A. Mahadevan-Jansen, S. L. Thomsen, G. Staerkel, A. Malpica, T. Wright, N. Atkinson and R. Richards-Kortum, "Cervical precancer detection using a multivariate statistical algorithm based on laser-induced fluorescence spectra at multiple excitation wavelengths," Photochem Photobiol, 64(4), 720-735 (1996)

38. N. Ramanujam, "Fluorescence spectroscopy of neoplastic and non-neoplastic tissues," Neoplasia 2(1-2), 89-117 (2000)

39. J. R. Lakowicz, "Introduction to Fluorescence," in Principles of Fluorescence Spectroscopy, pp. 1-26, Springer (3rd Edition), (2006).

40. J. R. Lakowicz, "Fluorophores," in Principles of Fluorescence Spectroscopy, pp. 63-95, Springer, (3rd Edition), (2006).

41. S. G. Demos, R. Bold, R. D. White and R. Ramsamooj, "Investigation of near-infrared autofluorescence imaging for the detection of breast cancer," Ieee J Sel Top Quant 11(4), 791-798 (2005)

42. X. Han, H. Lui, D. I. McLean and H. S. Zeng, "Near-infrared autofluorescence imaging of cutaneous melanins and human skin in vivo," Journal of Biomedical Optics 14(2), - (2009)

CHAPTER III

Near-Infrared Autofluorescence for the Detection of Parathyroid Glands

Constantine Paras,[1,*] Matthew Keller,[1] Lisa White[2], John Phay[3] and Anita Mahadevan-Jansen[1,4]

[1]*Department of Biomedical Engineering, Vanderbilt University, Nashville, TN 37235, USA*
[2]*Division of Surgical Oncology, Department of Surgery, Ohio State University, Columbus, OH 43210, USA*
[3]*Department of Surgery, Vanderbilt University, Nashville, TN 37232, USA*
[4]*Department of Neurological Surgery, Vanderbilt University, Nashville, TN 37232, USA*

[*]*Corresponding author: anita.mahadevan-jansen@vanderbilt.edu*

Introduction

Disease of the parathyroid and thyroid glands are common, with 25-28 cases per 100,000 of hyperparathyroidism and approximately 20 million people affected by some sort of thyroid disease (1, 2). Surgical means are used to remove the affected gland(s) when the disease cannot be treated by other methods (3). Endocrine surgery has traditionally involved meticulous dissection and resection of diseased glands while leaving the normal glands intact. Serious complications can occur when one or more of the parathyroid glands is unintentionally injured or removed during thyroidectomies or incompletely removed during parathyroidectomies (4). The incidence of inadvertent parathyroidectomy ranges from 8% to 19% in patients undergoing total thyroidectomy and depends of the level of experience of the surgeon (5). Such accidental removal or injury of the parathyroid may lead to complications such as postoperative hypocalcaemia and hypoparathyroidism that may have lifelong deleterious consequences on calcium homeostasis.

The parathyroid glands can be difficult to distinguish surgically because of their small size and appearance that is often similar to lymph nodes, fat and occasionally thyroid tissue. In addition, parathyroid identification is often confounded by variability in location of the glands and overlying layers of fat. Existing methods rely on histopathology or post-operative evaluation to determine if the parathyroids were accidentally or incompletely removed (6). Surgical biopsy of the parathyroid for identification can lead to devascularization and destruction of the functional gland; consequently, surgeons must ultimately rely on visual inspection to identify the different tissues, which can be subjective and inconclusive, especially for an inexperienced

surgeon (7, 8). In fact, thyroidectomies are typically performed by general or ear nose and throat surgeons, rather than endocrine surgeons, thus, an accurate, automated tissue identification method would allow safer, more effective patient management (9, 10).

The goal of this study then was to develop an optical method to intra-operatively discriminate parathyroid tissue from all other anatomical structures in the neck. This paper presents a method for identification of parathyroid tissue regardless of disease state based on intrinsic NIR autofluorescence. In a pilot study, data was collected *in vivo* from 21 patients undergoing surgery. In every patient, parathyroid tissue exhibited more intense autofluorescence above 800nm allowing us to distinguish it from the surrounding tissue.

Methods

Measurements were performed at the Vanderbilt University Medical Center under approval by the Vanderbilt Institutional Review Board. All patients with primary thyroid or parathyroid pathophysiology undergoing thyroid/parathyroidectomy were considered. Initial evaluation was conducted by the participating endocrine surgeon (Dr. John Phay) while seeing the patients at the Vanderbilt Clinic and final eligibility was determined preoperatively based on the clinical condition and safety of the patient. Twenty-one patients, aged 18-99, regardless of race and gender, were enrolled in the study following informed written consent.

Near infrared fluorescence was excited with a 785 nm diode laser (U-type, IPS, Monmouth Junction, NJ) that delivered 80 mW at the tissue surface with a spot size of

400 μm. Fluorescence spectra were detected using a fiber optic spectrometer (S2000-FL, Ocean Optics, Dunedin, FL) with a spectral resolution of 10.5 nm (FWHM). The entire system is computer controlled by custom software developed in LabView (National Instruments, Austin, TX). Light was delivered and collected from the tissue site with a 6-around-1 sterilized fiber optic probe. Inline filtering in the probe prevents 785 nm light from interfering with the collected fluorescence light (11). An additional 3 mm diameter longpass filter was placed in the fiber port of the spectrometer to further reduce the amount of 785 nm light entering the detector.

Fluorescence spectra were measured from multiple locations in the thyroid, parathyroid, fat, muscle and lymph depending on the accessibility of the tissues. All measurements were made with the room and operating lights turned off. The fiber optic probe was placed firmly in contact during each measurement while maintaining uniform pressure after removal of any excess blood that might be present at the investigated site. Background measurements were recorded with the laser turned off prior to measurements. Six spectra were acquired at each site with an integration time of 300 ms and averaged. In each case, visual inspection by the attending surgeon determined the tissue type corresponding to the acquired spectrum; the level of confidence in the surgeon's identification of each tissue was noted as high, medium or low. All sites rated as low confidence by the surgeon were excluded from analysis. Visual inspection therefore served as the gold standard of detection unless the investigated site was excised, in which case spectra were correlated with histology. In each of the 21 patients studied, histology was obtained from either the parathyroid or the thyroid, or both, depending on patient diagnosis and related surgical resection. In total, histology was obtained from 16

excised thyroid samples and 10 excised parathyroid samples and found to validate the anatomical identity of the measured gland.

Near-infrared fluorescence spectra were processed using MATLAB (Mathworks Inc., Natick, MA). First, background was subtracted and the data was corrected for the wavelength dependent response of the system with a National Institute of Standards and Technology (NIST) calibrated light source. Calibrated spectra were smoothed with a moving average filter of size 10 then normalized to the maximum intensity of the mean thyroid spectrum from that patient.

Results

In each patient, fluorescence from the parathyroid was compared to the fluorescence from the thyroid and other tissues in the neck. Figure 1a shows the NIR fluorescence spectra from a typical patient. The fluorescence intensity of the parathyroid was found to be the strongest among measured tissues. Further, thyroid fluorescence is observed to be

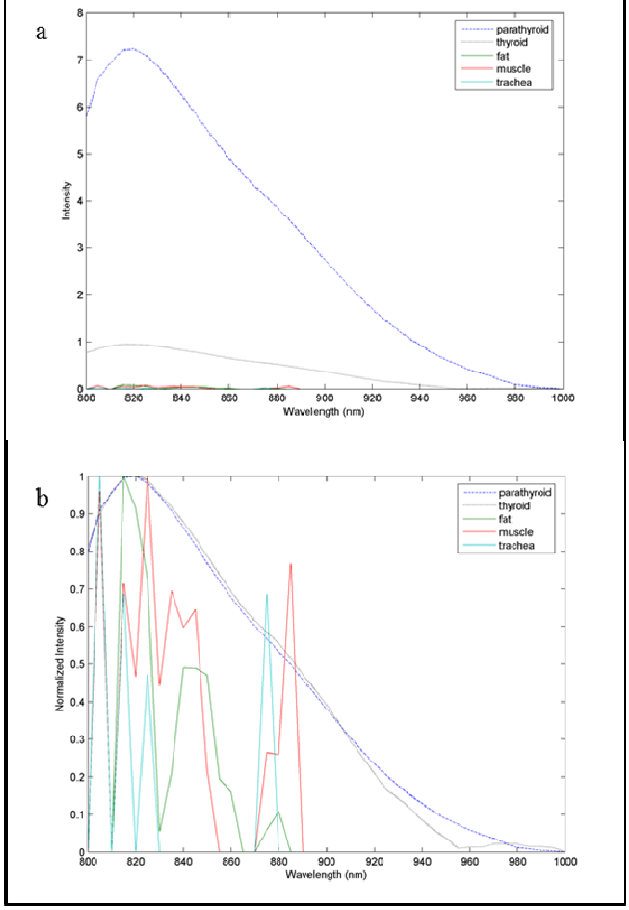

Figure 1: *(a) Fluorescence spectra measured from parathyroid, thyroid, fat, muscle and trachea of a typical patient. (b) Fluorescence spectra from parathyroid and thyroid tissue normalized to their respective peaks.*

stronger than surrounding muscle and fat but weaker than the parathyroid. Figure 1b presents the fluorescence spectra from parathyroid and thyroid tissues, normalized to their respective peak intensities demonstrating the similarity in their spectral lineshape. Since no fluorescence (intensity and lineshape above the level of noise) was measured from the muscle, fat and trachea, these signals were excluded from further analysis.

Average peak intensity for parathyroid fluorescence was consistently greater than that of the thyroid and other tissues in all 21 patients (fig. 2a). The *in vivo* parathyroid fluorescence was observed to be 2 – 11 times more intense than the thyroid fluorescence (fig. 2b). Analysis by student's t-test shows that the parathyroid exhibits more intense fluorescence than thyroid tissue with a p-value of .0000235 at a 99.9% level of significance indicating that the difference in intensity is statistically significant.

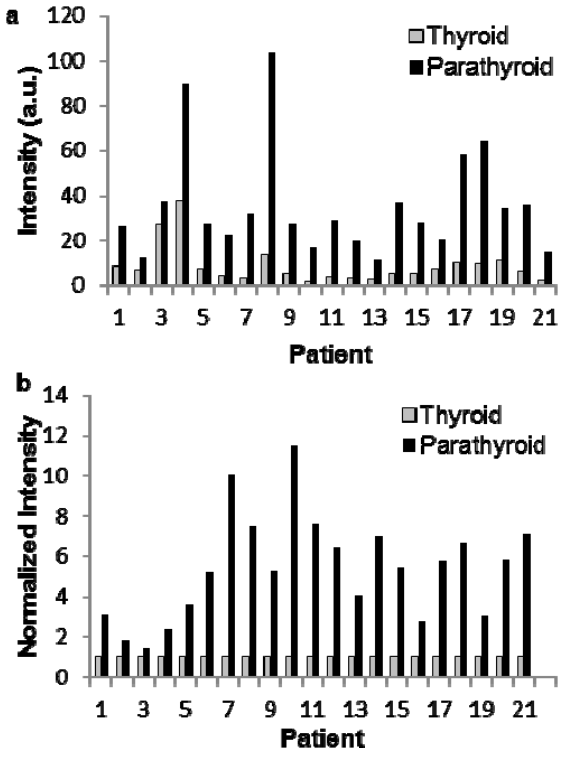

Figure 2: *(a) Average fluorescence peak intensity and (b) normalized peak intensity from parathyroid and thyroid measurements from each patient.*

Both parathyroid and thyroid histology was available in the same patient in 4 of the 21 cases studied due to concurrent disease. In these 4 patients, the fluorescence intensity of the parathyroid was found to be 2 - 10 times greater than that of the thyroid which is consistent with the observed results in the rest of the

patients. Thus, these 4 patients provide histological validation to the increased intensity of the parathyroid as compared to the thyroid. It should be noted that either parathyroid or thyroid histology was available in all other patients, confirming the anatomical identity of that gland. Spectra from glands that were not excised (where identification relied on visual inspection) were found to match the spectral characteristics of the histologically correlated parathyroid and thyroid autofluorescence signals.

The 21 patients enrolled in this study represent a variety of disease states. The first 7 patients in figure 2 were diagnosed with primary hyperparathyroidism, having either parathyroid disease (patients 1-3) or parathyroid disease with concomitant thyroid nodules or goiter (patients 4-7). The remaining 14 patients presented with thyroid disease and apparently normal parathyroids. In all 21 patients, the parathyroid fluorescence intensity was found to be consistently greater than that of the thyroid indicating that both normal and hyperfunctioning parathyroid tissue produce a much stronger fluorescence.

Discussion

Results presented here show that NIR fluorescence can successfully detect parathyroid tissue *in vivo*, in real-time and non-intrusively during endocrine surgery with near-perfect accuracy. This method improves on the sensitivity and specificity of visual recognition - a highly subjective measure that is dependent on the experience of the surgeon. More importantly, NIR autofluorescence can be used to identify parathyroid glands, regardless of thyroid or parathyroid disease. This is a major advantage over

current intra-operative localization methods such as radio-nucleotide uptake, ultrasound and iPTH assay, which are only effective when the parathyroid is hyper-active (9).

Tissue autofluorescence is typically observed in the ultraviolet-visible (UV/VIS) wavelength range (12). However, studies performed across multiple tissues in vitro (unpublished data) as well as in vivo (presented here) indicate that the near infrared spectra measured from thyroid and parathyroid tissues are repeatable (within the same tissue) and highly reproducible (across all patients) reinforcing the validity of the detected signal. The observed signal exhibits the typical Stokes' shift associated with fluorescence and the peak emission wavelength does not vary, indicating that this is a form of luminescence and is most likely due to tissue autofluorescence. Studies also show that the observed signal is not an effect of the system or its various components (13). In particular, changing the longpass filter does not affect the signal intensity or shape ruling out artifacts arising from the filters' transmission characteristics. Additionally, optical properties in this region of the spectrum were found to be fairly uniform between parathyroid and thyroid tissues indicating that the effect is not explained by differences in scattering or absorption. These observations lead to the conclusion that the signal is indeed due to tissue autofluorescence; the basis for this fluorescence is, however, presently unknown.

Near infrared wavelengths are considered the optical window and are attractive in biomedical applications due to their increased penetration depth and decreased scattering and absorption in tissues relative to UV/VIS wavelengths. This makes the NIR region optimal for biological studies spurring research efforts to use NIR wavelengths in the diagnosis and detection of disease (14). Research in NIR fluorescence has mostly

involved exogenous contrast agents, most commonly polymethines (15). Notably, indocyanines, such as indocyanine green (cardio-green) have been used extensively (15). However, contrast agents are difficult to translate to the clinic due to potential problems such as toxicity, photobleaching, and localization.

Autofluorescence uses biological fluorophores that occur naturally in tissues and thus negates the need for the introduction of exogenous agents, however, tissue typically exhibits peak autofluorescence in the UV/VIS wavelengths (400-700 nm) (12). Except, it is well documented in the Raman spectroscopy literature that tissue spectra measured at 785 or 830 nm excitation display residual broadband signal that is believed to be fluorescence background. Several groups have exploited this broadband signal to assist in the detection of a variety of pathologies ranging from cutaneous melanin in pigmented skin disorders to neoplastic breast tissue (16-19). The tissue autofluorescence in these studies was attributed to fluorophores such as melanin and porphyrins but none of these studies documented peak fluorescence in the NIR region (16-19).

Intrinsic biological fluorophores are typically reported to exhibit peak fluorescence below 800 nm of the NIR region (12). However, this paper clearly demonstrates the consistent presence of autofluorescence with peak emission at 820 nm in parathyroid and thyroid tissues. Das et al. used Raman spectroscopy to examine parathyroid pathology but used 830 nm excitation, thus missing the fluorescence peak (20). Since the peak fluorescence emission from the parathyroid and thyroid occurs at the same wavelength, it is hypothesized that the same fluorophore is responsible. Potential candidates are likely to be present in both the thyroid and parathyroid glands. The increased fluorescence in the parathyroid implies that they would occur in greater amounts or concentrations in the

parathyroid or that the fluorescence is somehow quenched in the thyroid. Porphyrins are known to be the longest emitting fluorophores in biological tissues with peak emission in the 600 – 700nm range, however, the fluorescence shown here has peak emission above 800nm (12). Melanin was hypothesized to be the primary contributor to the observed NIR autofluorecence in the eye and skin, but melanin is not known to be present in parathyroid and thyroid tissues (17, 18). A potential candidate based upon physiological examination is the calcium-sensing receptor present in both parathyroid and thyroid tissues but nowhere else in the neck. Ultimately, detailed analysis beyond the scope of this initial feasibility study will need to be performed to determine the responsible fluorophore(s).

Conclusion

In conclusion, this paper presents the potential of using NIR autofluorescence for the real-time anatomic guidance of endocrine surgery. Even though the basis for this fluorescence is not understood, the intensity of the measured signal allows for the feasibility of an imaging approach increasing the likelihood of its successful implementation in the operating room. Translation of this technology would reduce the rate of complications from accidental or incomplete removal of parathyroid tissue; anatomical guidance would also decrease operative time especially during lengthy parathyroidectomies where the surgeon must search for parathyroid glands.

References

1. L. Kim, M. W. Krause, V. Kantorvich, "Hyperparathyroidism," (G. T. Griffing – Editor), http://emedicine.medscape.com/article/127351-overview , (2011).

2. J. A. Sosa, N. R. Powe, M. A. Levine, R. Udelsman and M. A. Zeiger, "Profile of a clinical practice: Thresholds for surgery and surgical outcomes for patients with primary hyperparathyroidism: a national survey of endocrine surgeons," J Clin Endocrinol Metab 83(8), 2658-2665 (1998

3. G. Doherty, "Thyroid and Parathyorid," in Oncology: an evidence-based approach (A. E. Chang, P. A. Ganz, D. F. Hayes, T. Kinsella, H. I. Pass, J. H. Schiller, R. M. Stone, V. Strecher – Editors), Springer, (1st Edition) (2006).

4. ATA, "Thyroid Surgery," American Thyroid Association, http://www.thyroid.org/patients/brochures/ThyroidSurgery.pdf, (2005).

5. D. T. Lin, S. G. Patel, A. R. Shaha, B. Singh and J. P. Shah, "Incidence of inadvertent parathyroid removal during thyroidectomy," The Laryngoscope 112(4), 608-611 (2002)

6. A. Frilling and F. Weber, "Complications in Thyroid and Parathyroid Surgery," in Surgery of the Thyroid and Parathyroid Glands (D. Oertili, R. Udelsman – Editors), pp. 217-224, (1st Edition), (2007).

7. R. D. Bliss, P. G. Gauger and L. W. Delbridge, "Surgeon's approach to the thyroid gland: surgical anatomy and the importance of technique," World J Surg 24(8), 891-897 (2000)

8. F. R. Miller, "Surgical anatomy of the thyroid and parathyroid glands," Otolaryngologic clinics of North America 36(1), 1-7, vii (2003)

9. A. T. Ahuja, K. T. Wong, A. S. Ching, M. K. Fung, J. Y. Lau, E. H. Yuen and A. D. King, "Imaging for primary hyperparathyroidism--what beginners should know," Clinical Radiology 59(11), 967-976 (2004)

10. S. Fakhran, B. F. t. Branstetter and D. A. Pryma, "Parathyroid imaging," Neuroimaging clinics of North America 18(3), 537-549, ix (2008)

11. A. Mahadevan-Jansen, M. F. Mitchell, N. Ramanujam, U. Utzinger and R. Richards-Kortum, "Development of a fiber optic probe to measure NIR Raman spectra of cervical tissue in vivo," Photochem Photobiol, 68(3), 427-431 (1998)

12. J. R. Lakowicz, "Introduction to Fluorescence," in Principles of Fluorescence Spectroscopy, pp. 1-26, Springer (3rd Edition), (2006).

13. C. Paras, Keller M, White L, Whisenant J, Gasparino N, Phay J, Mahadevan-Jansen A, "Optical guidance of endocrine surgery (7169-59)," in SPIE Photonics West Bios, unplished conference proceedings SPIE, San Jose, CA (2009).

14. E. Tanaka, H. S. Choi, H. Fujii, M. G. Bawendi and J. V. Frangioni, "Image-guided oncologic surgery using invisible light: completed pre-clinical development for sentinel lymph node mapping," Ann Surg Oncol 13(12), 1671-1681 (2006)

15. J. V. Frangioni, "In vivo near-infrared fluorescence imaging," Current opinions in chemical biology 7(5), 626-634 (2003)

16. S. G. Demos, R. Bold, R. V. White and R. Ramsamooj, "Investigation of near-infrared autofluorescence imaging for the detection of breast cancer," Selected Topics in Quantum Electronics, IEEE Journal of 11(4), 791-798 (2005)

17. X. Han, H. Lui, D. I. McLean and H. Zeng, "Near-infrared autofluorescence imaging of cutaneous melanins and human skin in vivo," J Biomed Opt 14(2), 024017 (2009)

18. C. N. Keilhauer and F. C. Delori, "Near-infrared autofluorescence imaging of the fundus: visualization of ocular melanin," Invest Ophthalmol Vis Sci 47(8), 3556-3564 (2006)

19. X. Shao, W. Zheng and Z. Huang, "Near-infrared autofluorescence imaging for colonic cancer detection," in Optical Sensors and Biophotonics, pp. 76340B-76345, SPIE, Shanghai, China (2009).

20. K. Das, N. Stone, C. Kendall, C. Fowler and J. Christie-Brown, "Raman spectroscopy of parathyroid tissue pathology," Lasers in medical science 21(4), 192-197 (2006)

CHAPTER IV

Understanding the basis of the near infrared fluorescence found in parathyroid tissues

Constantine A Paras[1], Isaac J Pence[1], Chetan A Patil[1], John Phay[2], James Broome[3], Edward Brown, Anita Mahadevan-Jansen[1,4]

[1]*Department of Biomedical Engineering, Vanderbilt University, Nashville, TN 37235, USA*

[2]*Division of Surgical Oncology, Department of Surgery, Ohio State University, Columbus, OH 43210, USA*

[3]*Department of Surgery, Vanderbilt University, Nashville, TN 37232, USA*

[4]*Department of Neurological Surgery, Vanderbilt University, Nashville, TN 37232, USA*

[*]*Corresponding author: anita.mahadevan-jansen@vanderbilt.edu*

Introduction

The Endocrine system is a complex network within the body that primarily consists of ductless glands that secrete hormones into the blood stream to alter metabolic functions (1). Of these glands, the parathyroid glands are of vital importance for many bodily processes, such as hormone production and proper function of nervous and muscular systems. These glands are small, 6-8 mm long and 15-20 mg, with some variation in location which is dependent upon individual embryonic development. The average patient will have 3 to 5 parathyroid glands, generally in the neck near the thyroid gland which lies over the trachea and under the larynx. The tan coloration, small size, variable location, and potential inclusion within the thyroid gland increase the difficulty of locating the parathyroid gland during Endocrine surgery. The parathyroid glands produce and secrete Parathyroid Hormone (PTH), which is responsible for control of calcium hemostasis and constitutes the only mechanism to raise blood calcium levels. A lack of PTH would cause an inability to induce action potentials and lead to eventual death.

Disease of the parathyroid and thyroid glands can lead to a complex combination of conditions from fields of endocrinology and oncology (2). Cases of thyroid cancer and hyperparathyroidism often require surgery when alternative treatments fail. The primary complications in endocrine surgery occur during parathyroidectomy and thyroidectomy procedures. Parathyroidectomy is generally characterized by long surgical times and can result in incomplete removal of a parathyroid gland leading to a secondary surgery for persistent symptoms. During thyroidectomy procedures, accidental removal or damage to the parathyroid glands, or the failure to leave an adequate blood supply to the glands can

lead to hypoparathyroidism. This disorder has been variably reported in 2-50% of thyroidectomy procedures (3-5). The prevalence is directly proportional to a surgeon's experience and accounts for the major source of mortality and malpractice for endocrine surgical procedures. Furthermore, patient quality of life can be affected, requiring calcium and vitamin D supplements for the rest of their life and potential hypocalcemia symptoms of swelling of limbs, gastrointestinal (GI) discomfort, cataracts, and increased bone metabolism.

Current techniques to localize the parathyroid glands are all based on preoperative imaging. Ultrasound, CT, MRI and radionucleotide methods each offer potential benefits but are all plagued by high false-positive rates, can only be used with parathyroid disease, potential exposure to ionizing radiation, and ultimately still rely on visual recognition of the gland structure. Thus, there is a distinct need for a real-time and intra-operative system that is highly accurate and can provide feedback to a surgeon during endocrine procedures to locate the parathyroid glands.

Previous studies have indicated that an optical solution may exist for real-time anatomical detection of the parathyroid. The parathyroid and thyroid tissues demonstrate a consistent and repeatable near-infrared (NIR) autofluorescence signal. The peak fluorescence from the tissues is emitted above 800nm. Using 785nm excitation, a point-based fiber optic probe fluorescence spectroscopy system provided consistent and accurate performance across all patients (N=44). Compared with other tissues in the neck, only parathyroid and thyroid tissues exhibited NIR fluorescence, and the parathyroid signal is between 2 and 30 times stronger than that of the thyroid (6).

The consistent presence of the autofluorescence signal above 800nm has sparked examination of potential sources for a biological basis for the observed signal. Biological fluorophores naturally occurring in tissue typically exhibit peak autofluorescence in UV/VIS wavelengths (7). Aside from reports of melanin autofluorescence signal near 900 nm, there are no reports of other fluorophores endogenous to tissue with emission maxima in the NIR region (8).

There are a number of criteria that potential tissue components must meet to act as the differential source of autofluorescence. Based on the studies conducted thus far, the fluorophore must exhibit an emission peak of ~820 nm, must be present in significantly high quantities in the parathyroid with small to moderate quantities in the thyroid and none in the surrounding other tissues in the neck. Since no melanin is present in this area of the body, potential candidates include the various forms of porphyrins and the parathyroid hormone. However, the PTH hormone exhibited no fluorescence in the NIR and porphyrin peaks were identified to be at shorter wavelengths than was observed in

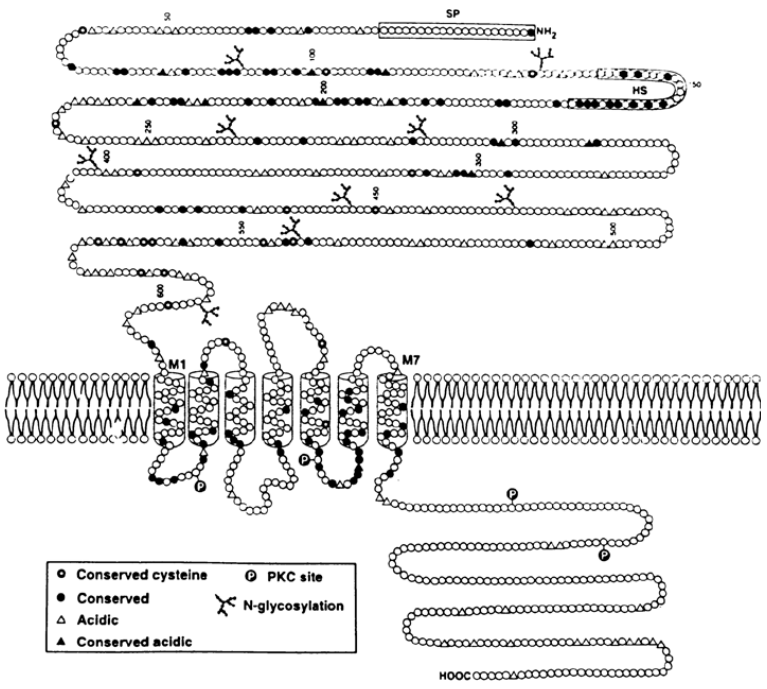

Figure 1: *Proposed structural model of the predicted bovine parathyroid Ca^{2+}-sensing receptor protein*

these studies. We therefore hypothesize that Calcium Sensing Receptor (CaSR), a large transmembrane receptor, acts as the endogenous fluorophore responsible for the observed signal. CaSR is involved in controlling the synthesis and secretion of PTH and calcitonin and is most abundant in the parathyroid. It is present to a lesser extent in C-cells of the thyroid. This receptor is also widely expressed in other tissues, including specific cell types within the kidney, osteoblasts, hematopoietic cells in bone marrow, GI mucosa, and squamous cells of the esophagus. In disease, CaSR is shown to activate mutations leading to disorders with hypocalcemia and neonatal hyperparathyroidism making it a viable candidate as the potential fluorophore responsible for the signals observed in this project.

The goal of this chapter therefore was to characterize the fluorescence and optical properties of thyroid and parathyroid tissues in order to validate the excitation-emission maxima as well as absorption and scattering properties of the potential fluorophore. This evaluation would further allow the identification of the optimal excitation wavelength for the instrument. Next the in vivo fluorescence signatures were evaluated to assess the effect of disease on the emission intensity of the parathyroid to further elucidate the contributor of this signal and the consistency of the observed signal was validated. Finally, the potential of CaSR as the contributing fluorophore was evaluated by assessing the fluorescence of other tissues where these receptors might be present (or absent).

In vivo NIR fluorescence properties

Measurements were performed at the Vanderbilt University Medical Center under approval by the Vanderbilt Institutional Review Board. All patients aged 18-99, regardless of race and gender, with primary thyroid or parathyroid pathophysiology undergoing thyroid/parathyroidectomy were considered. Initial evaluation was conducted by the participating endocrine surgeon (Dr. John Phay) at the Vanderbilt Clinic and final eligibility was preoperatively determined based on the clinical condition and safety of the patient. Twenty-one patients were enrolled in the study following informed written consent.

Near-infrared fluorescence was excited with a 785-nm diode laser (U-type, IPS, Monmouth Junction, New Jersey) that delivered 80 mW at the tissue surface with a spot size of 400 μm. Fluorescence spectra were detected using a fiber optic spectrometer (S2000-FL, Ocean Optics, Dunedin, Florida) with a spectral resolution of 10.5 nm (FWHM). The entire system is computer controlled by custom software developed in LabView (National Instruments, Austin, Texas). Light was delivered and collected from the tissue site with a 6-around-1 sterilized fiber optic probe. Inline filtering in the probe prevents 785 nm light from interfering with the collected fluorescence light (9). An additional 3-mm diameter longpass filter was placed in the fiber port of the spectrometer to further reduce the amount of 785 nm light entering the detector.

Fluorescence spectra were measured from multiple locations in the thyroid, parathyroid, fat, muscle, and lymph depending on the accessibility of the tissues. All measurements were made with the room and operating lights turned off. The fiber optic probe was firmly placed in contact during each measurement while maintaining uniform pressure after removal of any excess blood that might be present at the investigated site.

Background measurements were recorded with the laser turned off prior to each tissue measurement. Six spectra were acquired at each site with an integration time of 300 ms and averaged. In each case, the tissue type assigned to each acquired spectrum was visually determined by the attending surgeon; the level of confidence in the surgeon's identification of each tissue was noted as high, medium, or low. All sites rated as low confidence by the surgeon were excluded from analysis. Visual inspection therefore served as the gold standard of detection unless the investigated site was excised, in which case spectra were correlated with histology.

Near-infrared fluorescence spectra were processed using MATLAB (Mathworks Inc., Natick, Massachusetts). First, background was subtracted and the data was corrected for the wavelength dependent response of the system with a National Institute of Standards and Technology calibrated light source. Calibrated spectra were smoothed with a 10-point moving average filter and then normalized to the maximum intensity of the mean thyroid spectrum from that patient.

Analysis

A comparison of the fluorescence spectra acquired from the different tissues in the neck showed that fluorescence emission was consistently observed at 822 nm in the thyroid and parathyroid tissues; no measurable signal was measured from all other tissues (Figure 2). The peak was found to

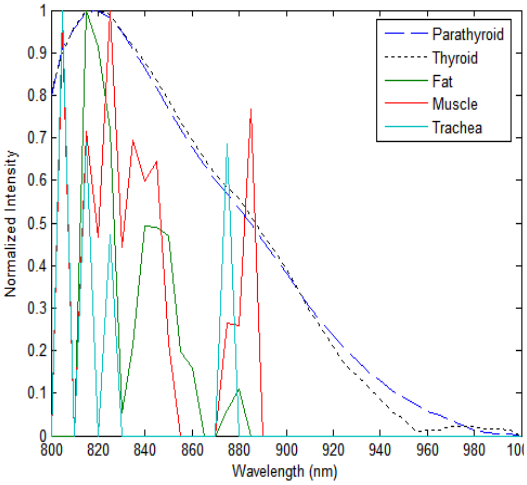

Figure 2: *Normalized fluorescence from various tissues in the neck.*

be repeatable within the same tissue and consistent across different patients. Further, in each of the 44 patients studied, histology was obtained from either the parathyroid or the thyroid, or both, depending on patient diagnosis and related surgical resection. In total, histology was obtained from 16 excised thyroid samples and 10 excised parathyroid samples and found to validate the anatomical identity of the measured gland.

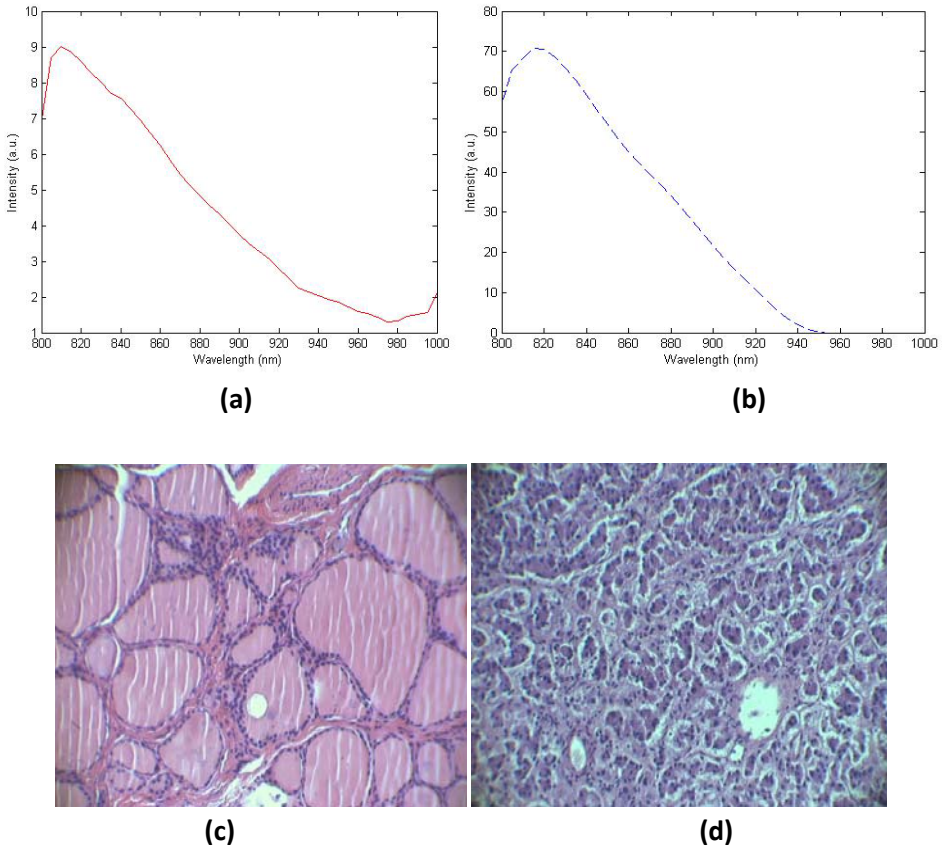

Figure 3: *Fluroescence spectrum of the (a) thyroid. And (b) Parathyroid. (c) Histological confirmation of thyroid tissue and (d) parathyroid tissue.*

Average peak intensity for parathyroid fluorescence was consistently greater than that of the thyroid and other tissues in all 44 patients. Analysis by student's t-test shows that the parathyroid exhibits more intense fluorescence than thyroid tissue with a p-value of 0.0000235 at a 99.9% level of significance indicating that the difference in intensity is

statistically significant. A receiver-operator characteristic (ROC) curve was plotted to compare the ability to detect the parathyroid by autofluorescence in comparison to other methods such as ultrasound, sestamibi and CT. Figure 4 shows the ROC curve obtained. The figure clearly presents the superior identification using fluorescence as compared to these other methods. At the current study power, this technique has 100% classification accuracy, with higher sensitivity and specificity than all other parathyroid gland localization techniques currently used (10-18).

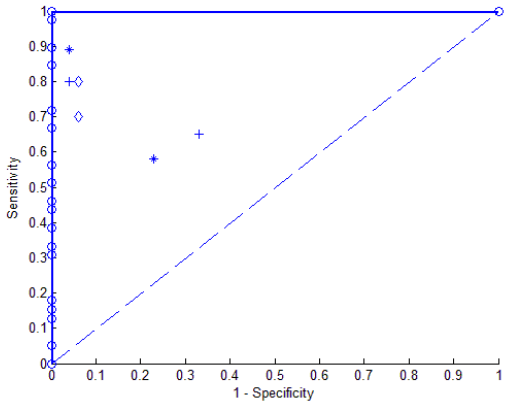

Figure 4: *Receiver Operator Characteristic comparing NIR fluorescence to other techniques: Ultrasound (+), sestamibi (*), and CT (◊). Area under ROC curve (AUC) for NIR fluorescence is 1.*

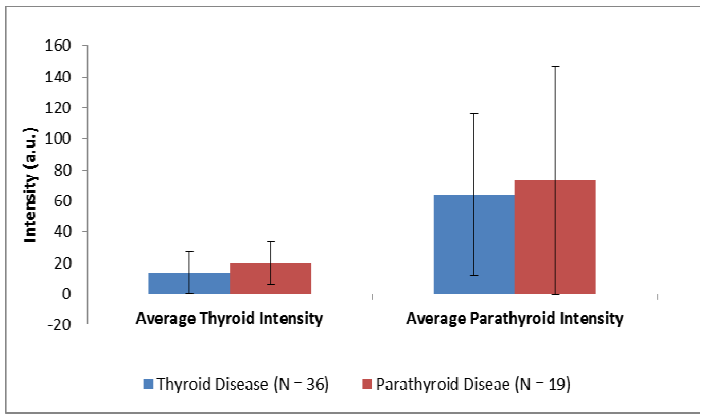

Figure 5: *Average peak fluorescence intensity of the thyroid and parathyroid gland in the presence of disease.*

Further the variability of the observed signal was compared as a function of disease state of the parathyroid and thyroid. Figure 5 demonstrates that the strong signal in the parathyroid glad was observed regardless of the disease state of the parathyroid. Similarly, the intensity of the thyroid signal did not vary with thyroid disease. Therefore, autofluorescence is capable of

detecting normal parathyroid glands, unlike currently available techniques applicable to diseased or hyperfunctioning glands.

Analysis of variance (ANOVA)

Reports have been made that optical signals are influenced by factors inherent to biological tissues (19, 20). To determine whether the observed autofluorescence signal was affected by systematic inter-patient variations, ANOVA was performed separately for parathyroid and thyroid data with factors such as disease source, gender, and age. As seen in Table 1, no significant differences were found as a function of age or gender with averaged parathyroid intensities. For analysis using normalized intensities, the result was less significant. The large within-group variance can be accounted for by the large patient-to-patient differences and may be improved with increased sample size.

In order to determine the tissue component(s) responsible for the generation of the autofluorescence and to more fully understand the difference in signal strength, it is necessary to measure the intrinsic optical properties of the tissues of interest.

Table 1. *ANOVA Results: Average Parathyroid Intensity*

Source of Variation	***SS***	***Df***	***MS***	***F***	***P-value***	***F crit***
Between Groups	31372.49	10	3137.249	0.771026	**0.65632**	1.909792
Within Groups	492340.2	121	4068.927			
Total	523712.7	131				

Optical properties

Method

In order to better characterize the optical signal detected in the clinical studies, the optical and fluorescent properties of bulk thyroid and parathyroid tissues were measured in the Biomedical Photonics Laboratories at Vanderbilt University under a protocol approved by the Vanderbilt University Medical Center Institutional Review Board. Bulk tissue specimens of healthy thyroid and parathyroid tissue were obtained fresh, frozen and prepared for optical measurement by placing the tissue between two fused silica glass slides. Transmission and reflectance measurements were collected in the near-infrared (NIR) using a spectrophotometer (Perkin-Elmer, Lambda 900). Measurements were collected from 700 to 900 nm. Optical absorption (μ_a) and reduced scattering (μ_s') coefficients were calculated using the inverse adding-doubling algorithm (21). Fluorescent properties were also measured using a spectrofluorometer (Photon Technology International, Xenon continuous wave lamp, photomultiplier detection). Excitation-emission matrices (EEM's) were created in the NIR with excitation wavelengths ranging from 690 to 825 nm in 5 nm increments, and emission wavelengths detected from 700 to 1000 nm in 1 nm increments. Measurements consisted of an average of two 0.5 s acquisitions.

Analysis

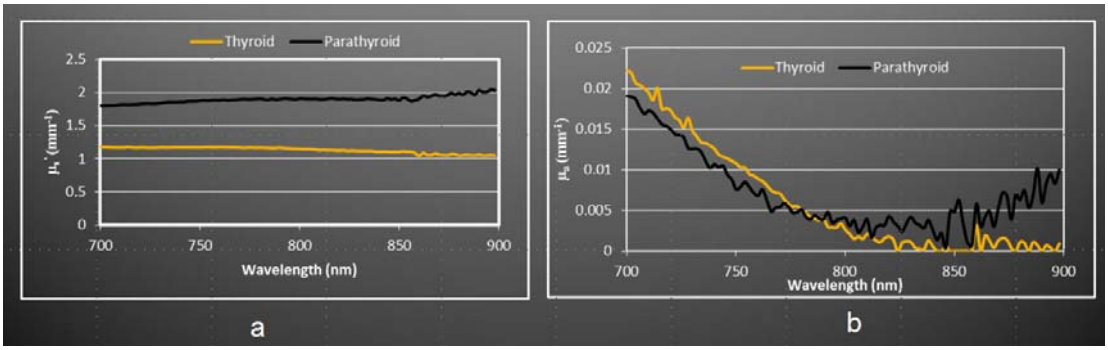

Figure 6: *(a) Reduced scattering, μ_s' spectra and (b) absorption spectra of thyroid and parathyroid tissue from 700 – 900 nm.*

The reduced scattering coefficient, μ_s', of both the thyroid and parathyroid is fairly constant over the 700-900 nm wavelength range (Figure 6a). Parathyroid exhibits greater scattering, with a $\mu_s' \approx 2$ mm^{-1} across this entire wavelength range. Thyroid scattering is lower, at $\mu_s' \approx 1.1$ mm^{-1}. The absorption coefficient of both thyroid and parathyroid is approximately equal across the NIR (Figure 6b). Absorption decreases linearly from $\mu_a \approx 0.02$ mm^{-1} at 700 nm to less than $\mu_a \approx 0.005$ mm^{-1} at 800 nm. Parathyroid absorption increases slightly starting at 860 nm up to $\mu_a \approx 0.01$ mm^{-1} at 900 nm.

EEM

The thyroid NIR EEM is shown in Figure 7a. Figure 7b is a plot of the thyroid emission spectrum when excited at 785 nm, and clearly shows the strong emission peak at 822 nm. Autofluorescence emission at 822 nm generally increases with longer excitation wavelengths, as seen in Figure c. The EEM clearly illustrate the presence of the 822 nm emission peak regardless of NIR excitation wavelength, as well as the general increase in emission intensity at longer wavelengths.

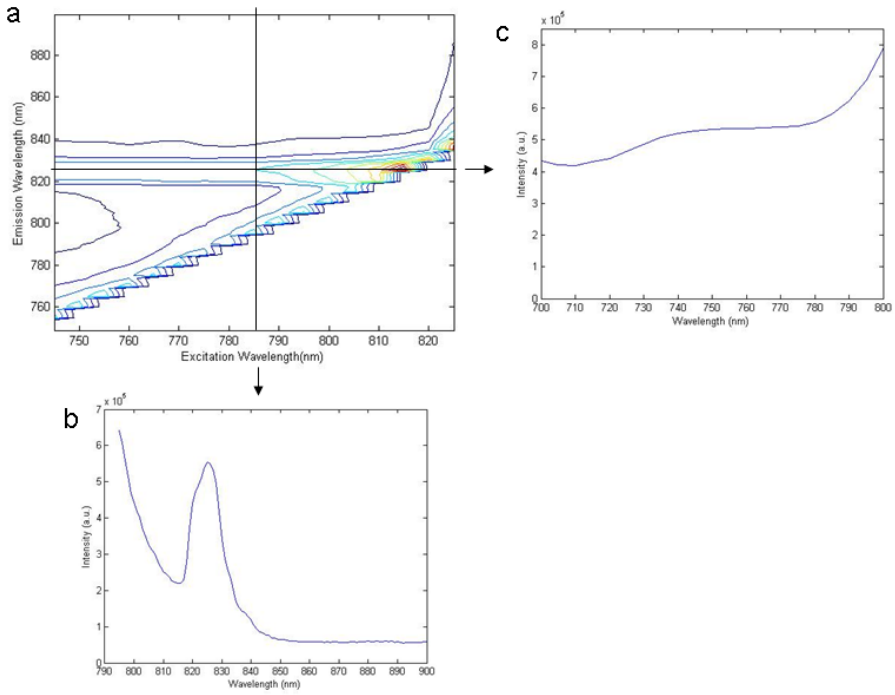

Figure 7: *Excitation emission matrix of the thyroid.*

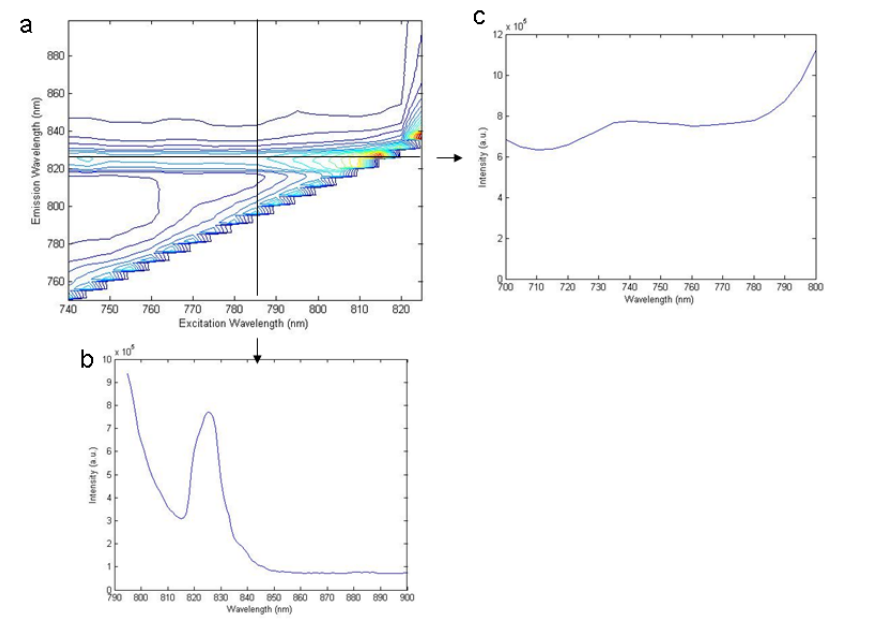

Figure 8: *Excitation emission matrix of the parathyroid.*

The parathyroid NIR EEM is shown in Figure 8a is a plot of the parathyroid emission spectrum when excited at 785 nm. Again, the presence of a single, prominent emission

peak at 822 nm is clear. Parathyroid autofluorescence emission at 822 nm (Figure 8c) is also similar to the thyroid, and generally increases with longer excitation wavelengths.

Molecular basis of NIR fluorescence

The presence NIR autofluorescence signal in the thyroid and parathyroid tissues poses an interesting question that currently has no explanation. The potential biological constituents which account for the detected signal must have a higher concentration in the parathyroid and a reduced concentration in the thyroid (or is somehow quenched in the thyroid). These same tissue components should also not be present in the other tissue types found in the neck cavity as no detected autofluorescence signal was observed in them. Examination of physiological and biological properties of the tissues of interest suggests that potential sources of this autofluorescence include parathyroid hormone (PTH), various forms of porphyrins, and calcium sensing receptors (CaSR).

The parathyroid glands are responsible for the production of Parathyroid Hormone (PTH), the principal regulator of calcium within the human body. These minute glands are of great importance as plasma calcium levels require tight regulated and have a role in neuromuscular excitability, excitation-contraction coupling in both cardiac and smooth muscle cells, stimulus-secretion coupling functions, maintenance of tight-junctions, and blood-clotting.[1] In order to maintain the body's ability to create heart contractions, PTH ensures constant plasma calcium levels by mobilizing calcium from bone fluid, stimulating calcium conservation in the kidneys and activating vitamin D in the intestines, resulting in an increased reabsorption of calcium and phosphate. Figure 12

shows a diagram of the physiological interactions responsible for the regulation of plasma calcium. Due to the necessity for constant and precise regulation of plasma calcium levels, both the superior and inferior parathyroid glands receive a rich supply of blood via the inferior thyroid artery.[2] Such strict control of plasma calcium level necessitates properly functioning parathyroid glands for a person's well-being and survival.

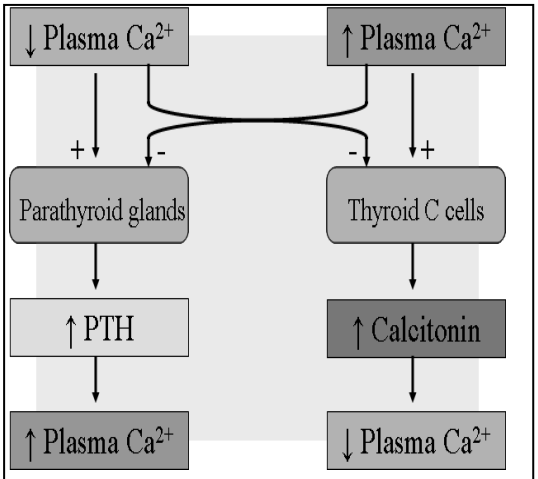

Figure 9: *Negative-feedback loops controlling calcitonin and Parathyroid Hormone (PTH) secretion*

While PTH makes for the most viable candidate for the observed fluorescence, it is unique to the parathyroid, and is found in no other tissues within the neck region including the thyroid. Furthermore, hyperfunctioning parathyroid tissue does not exhibit increased signal and *in vitro* studies found no fluorescence signal associated with PTH, discrediting it as a potential fluorophore. Porphyrins are known as the longest emitting fluorophores in biological tissues, with peak emissions in the 600-700nm range (7). However, there are no reports of porphyrins as tissue components in the thyroid or parathyroid glands, decreasing their likelihood as the fluorophore of interest.

We therefore, hypothesize that CaSR acts as the endogenous fluorophore responsible for the observed signal. Calcium-sensing receptors are ;arge amino acids involved in controlling synthesis and secretion of PTH and calcitonin. They are unique and share sequence and topology similar only to the metabotropic glutamate receptors (18 – 24% identity overall) and no other G protein-coupled receptors (22). Together these

receptors form a novel subfamily within the G protein-coupled receptors possibly explaining why this effect has not been previously reported.

The highest levels of CaSR expression are found in parathyroid cells (23-25). The CaSR is also present in smaller concentrations almost exclusively in the C-cells of the thyroid (which comprise roughly 5% of the gland) but nowhere else in the muscle, fat or lymph of the neck region (26). This provides a fluorophore that is present in high concentrations in parathyroid tissue and low concentrations in thyroid tissue making CaSR a highly probable candidate for the observed fluorescence.The calcium-sensing receptor can also be found in most of the renal tubule and is present at the highest levels in the cortical thick ascending limb of the nephron, brain, bone and epithelial lining of the colon. If our hypothesis is correct, then these tissues expressing CaSR should display a NIR fluorescence signal as well.

Evidence that CaSR is the source of the autofluorescence signal observed in the thyroid and parathyroid was gathered by acquiring optical measurements from other tissues known to express CaSR as well as from tissues with pathological conditions known to affect CaSR expression. Analyzing and comparing the autofluorescence signal from parathyroid, thyroid, kidney and colon tissues may yield useful information about the status of CaSR as the potential fluorophore candidate, as well as comparing the results of disease models that are reported to effect expression has the potential to yield further useful information. Hyperparathyroidism is one such condition in which there is variable down-regulation of CaSR reported in 35-76% of cases (27). Wilm's tumor, a particular type of cancer found in the kidney is another disease model, where CaSR is

down-regulated. These tissues and disease model may also be examined to further evaluate CaSR as a potential fluorophore of interest in this project.

Tissue NIR fluorescence

The impact of hyperparathyroidism on the autofluorescence signal was analyzed using data collected from the in vivo study plus which includes 57 patients in all. The data was partitioned into cases of thyroid disease (n=36) and parathyroid disease (n=19). Student's t-test for two samples was used to analyze the data for differences between peak intensity for cases of thyroid disease compared with those of parathyroid disease. Figure 6 shows the comparison of the peak intensities. When including all cases both raw and normalized data found no significant evidence of difference ($p>0.05$). Review of the data found cases that were significant outliers were exerting influence on the statistical model. When these cases were removed and the analysis was rerun significant differences were found for the normalized data at $p=0.00226$. For the comparison of raw data between diseases after removing the influential observations, the data was not significantly different between groups, confounding simple interpretation. A summary of the raw data can be found in Table 2, while Table 3 reports the data after influential outliers are removed. The comparison of group means when including all cases to those of removing the outliers and the p-values for the normalized data is summarized in Table 4. The significant change associated with 3 influential observations is found when comparing the normalized results, but further analysis of differences within the raw data remains.

Table 2: *Summary of all cases for disease groupings*

Source of Disease	Average Thyroid Intensity	Average Parathyroid Intensity	Normalized Parathyroid Intensity
Thyroid Disease (N = 36)	13.8745	63.93011	4.607742
Parathyroid Disease (N = 19)	19.6608	72.974	3.71165

Table 3: *Summary of disease groupings after removing influential observations*

Source of Disease	Average Thyroid Intensity	Average Parathyroid Intensity	Normalized Parathyroid Intensity
Thyroid Disease (N = 35)	14.2545	64.1386	4.499533
Parathyroid Disease (N = 17)	20.8924	56.4419	2.701552

Table 4: *Ratios of normalized parathyroid signal to thyroid signal and resulting p-values*

Normalized PT	All included	Outlier Removed
Thy Disease	4.6077	4.5
PT Disease	3.7117	2.7015
p-value	0.5401	0.00226

To further examine the potential of CaSR as the NIR fluorophore of interest, fresh, frozen Wilms' Tumor samples, a disease model of fetal kidney, were acquired from the Department of Pediatric Surgery and compared to normal tissue samples from the Vanderbilt-Ingram Cancer Center tissue bank after IRB approval. Prior to measurement with instrumentation and parameters used for the *in vivo* study of parathyroid and thyroid tissues, the samples were thawed in phosphate-buffered saline until approximately room temperature, then placed on a non-fluorescent background and

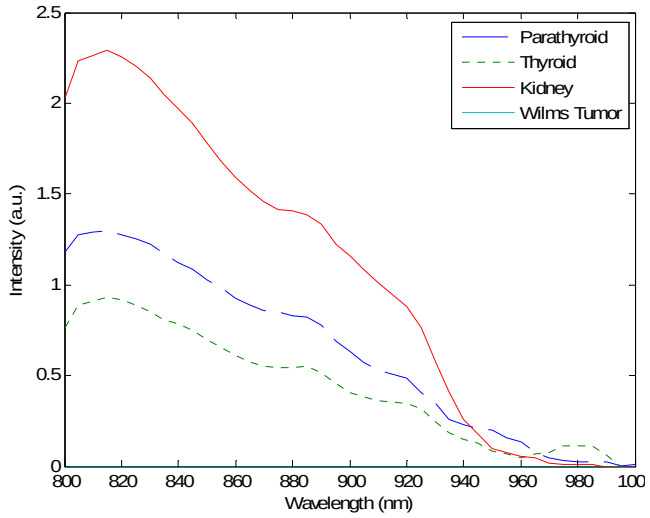

Figure 10: *NIR Fluorescence spectra of CaSR model tissues. Wilm's Tumor is expected to have reduced signal compared with healthy kidney samples based on the down-regulation of CaSR expression.*

measured with the fiber optic probe. The obtained autofluorescence signal for the Wilm's Tumor compared with that of Thyroid, Parathyroid, and normal Kidney are presented in Figure 13. The signal from the tumor samples was absent when processed and normalized when compared to the other tissue samples tested. These results are promising as CaSR is known to be down-regulated in Wilm's tumor as compared to normal kidneys. These results need to be validated using a sufficiently powered study.

Since CaSR is known to be intrinsically present in normal colon and kidney tissues, bulk colon and kidney tissue specimens were obtained from the Vanderbilt Tissue Bank for measurement of NIR autofluorescence. Tissue samples were flash frozen in liquid nitrogen and thawed to room temperature prior to optical measurement. All measurements were made under protocol approved by the Vanderbilt University IRB. Characterization of fluorescence signal was initially performed with the 785 nm NIR autofluorescence system previously used for clinical measurements of thyroid and parathyroid autofluorescence. NIR EEMs of the tissue specimens were also collected using a spectrofluorometer (Photon Technology International, Xenon continuous wave lamp, photomultiplier detection) with excitation wavelengths ranging from 690 to 825 nm in 5 nm increments, and emission wavelengths detected from 700 to 1000 nm in 1 nm increments. Measurements consisted of an average of two 0.5 s acquisitions.

Figure 11a is a comparison of the NIR autofluorescence of the colon with spectra obtained from the thyroid and parathyroid. The observed peak intensity is much lower than the parathyroid and on par with that from thyroid tissues. A noticeable local maximum near 822 nm is observed. A similar comparison of the NIR autofluorescence of the kidney specimens (Figure 11b) shows a strong autofluorescence peak at 822 nm.

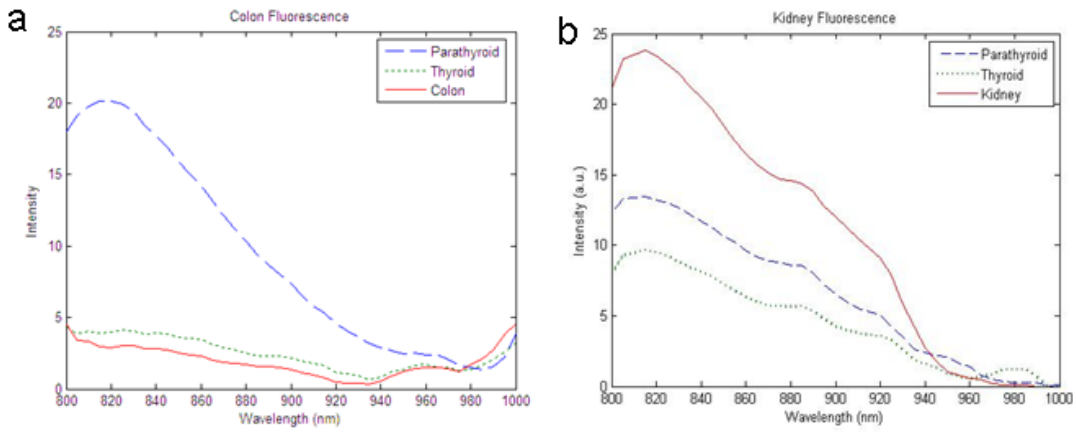

Figure 11: *NIR fluorescence spectra from normal (a) Colon and (b) Kidney.*

Further, EEMs were acquired for both the colon (Figure 12a) and the kidney (Figure 12b) in an effort to confirm that the optical signatures observed were the result of fluorescence emission similar to that observed in the parathyroid. The data collected also shows a clear emission maximum at 822 nm with increasing emission as the excitation

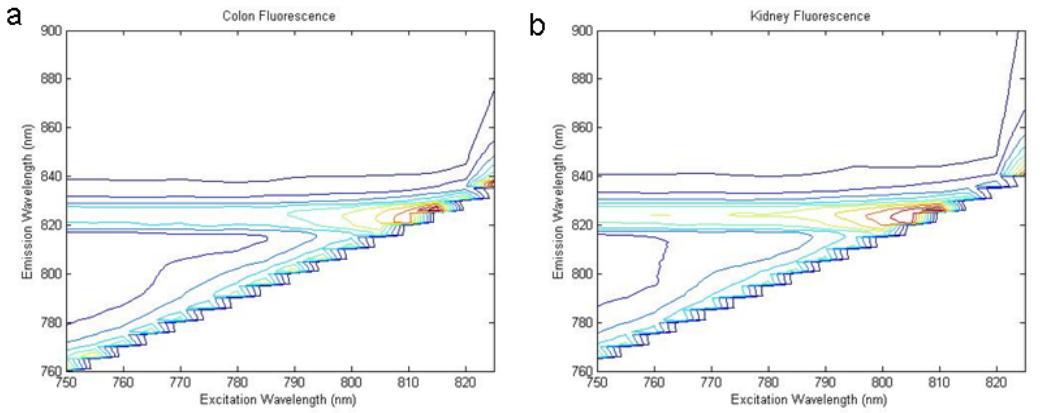

Figure 12: *EEM of (a) Colon Tissue and (b) Kidney Tissue.*

Discussion

Based upon observations shown in Chapter 3, the elevated fluorescence signal of the parathyroid gland compared to other tissues in the neck was studied *in vivo* using fiber optic probe-base fluorescence spectroscopy. The consistent and highly repeatable differences between the measured tissues are of great interest to endocrine surgeons who may be able to utilize this phenomenon for anatomical guidance and gland localization in real-time during procedures. The unexpected signal intensity from the parathyroid gland compared with other tissues in the same region poses many interesting questions. Since melanin, the only fluorophore known to emit above 800nm found in biological tissue, is not present in the thyroid or parathyroid, a new mechanism to explain the signal must be found. Even without a thorough understanding of the signal source, the results of the *in vivo* study are clear. The autofluorescence signal generated is variable between patients, but parathyroid is consistently stronger than that of the thyroid between 2 and 35 times. Both signals have the same underlying waveform, which may suggest a common underlying source of signal. The results were consistent even when filtering and other instrumentation specifics were changed over the course of the study, further suggesting the presence of an unexplained biological mechanism.

The classification performance of this technique based upon the *in vivo* data is unparalleled by other modern detection techniques for localizing the parathyroid glands. Unlike these other methods which are insensitive to normal glands and are either preoperative or low resolution, autofluorescence detection has been demonstrated *in vivo* in real-time. Furthermore, across 57 cases, the classification accuracy is 100%, without accounting for patient variables that may affect signal variability like age, gender, and

presence of disease. Classification performance should be further evaluated with an increased sample size, allowing for an appropriately powered study of multiple disease groups, genders, and ages for a parametric analysis. It is possible that within the data obtained, there are systemic changes that we have not been able to discern between certain patient groups. Regardless of the potential differences between patients, the measured signal is consistent and the difference great enough to merit further development of this technology and exploration of the underlying mechanism.

Even when the *in vivo* dataset was partitioned into diseases of the thyroid and parathyroid, there was no detected change in the autofluorescence peak location or intensity. These results imply that the underlying mechanism by which we are distinguishing these tissues is not affected by tissue disease. From 44 patients, 84 parathyroid glands were measured, 18 of which were abnormal and 66 normal. By analyzing the gland data as opposed to a patient peak intensity and removing influential observations, there is a significant difference in the intensity of signal between the normal and abnormal parathyroid tissues ($p<0.05$). Even with this change in intensity, there is still no report of a change in peak location. As fluorescence spectroscopy generally distinguishes between tissues when altered absorption, scattering, or fluorescence properties of the endogenous biomolecules and tissue structures change with pathology, it is unconventional that no signal difference is detected when disease is present. These findings would seem to suggest that the fluorophore responsible for the generation of the signal is either a biomolecule or structure that is not affected by the diseases or that the signal is strong enough that the change in tissue properties consistent with disease does not affect detection.

Measurement of the absorption and reduced scattering coefficients was an important step for characterization of the optical signals observed in the clinical measurements. Table 5 is a compilation of the optical properties of the thyroid and parathyroid we have measured along with optical properties of tissues encountered during thyroid surgery (28).

Table 5: *Optical Properties of Tissues in the Neck*

Tissue	μ_s' (mm^{-1})	μ_a (mm^{-1})
Skin	1.2-1.3	0.015-0.02
Fat	1.2	0.002-0.003
Muscle	0.5-0.6	0.00-0.04
Thyroid	1.16	0.004
Parathyroid	1.9	0.004

The optical properties of the thyroid and parathyroid are on the same scale as other tissues in the neck, and the dramatic differences observed in the clinical data cannot be explaind by differences in the optical properties alone. The moderate difference in scattering between the parathyroid and the thyroid may result in greater parathyroid diffuse reflectance. However, the signal observed in the *in vitro* and *in vivo* measurements is stokes' shifted from the excitation, which implies that the origin of the signal is autofluorescence. The absorption spectra of parathyroid and thyroid are nearly identical, and the spectral band where differences are observed (> 860 nm) does not overlap with the band where differences are observed in the clinical measurements. Although the optical absorption of both parathyroid and thyroid are fairly low in

comparison to other tissues in the neck, their similarity with one another does not indicate that measurements of optical properties alone could produce signals distinct enough to differentiate tissue types.

Collection of EEM for thyroid and parathyroid tissues verify the emission observed in the fiber optic probe based measurements, and confirm that autofluorescence is indeed the optical origin of the signal. The appearance of the emission peak at 822 nm with NIR excitation from 740 to 820 nm for both the thyroid and the parathyroid suggests that the same fluorophore is present in both tissues. There are, to our knowledge, no existing reports of endogenous tissue fluorophores with emission maxima near 822 nm. In an effort to thoroughly characterize fluorescence from the thyroid and parathyroid, EEMs were also collected. Regardless of the origin of the optical signal, the EEM data provides valuable data for optimizing the optical design for efficient measurement of parathyroid NIR fluorescence. The general increase in emission intensity with excitation from 740 to 820 nm explains the promising clinical results obtained using 785 nm excitation, and indicates that the use of longer excitation wavelengths, such as with the commonly available 808 nm diode source may benefit fluorescence yield and improve signal-to-noise. Detection of fluorescence emission could also be simplified and the instrumentation complexity could also be significantly reduced by employing a single photodiode for detection with a filter set designed to maximize collection near the 822 nm emission maxima. Moving forward, identification of the molecular origin of the optical signal will allow an improved understanding of the physiological origin of the signal, facilitate a better understanding of biological sources of signal variability, and

potentially to open the door to applications related to specific pathological conditions in the thyroid and parathyroid, as well as forms of tissue pathology in other tissue types.

The fluorescence emission spectra and EEMs obtained from colon and kidney tissues support the hypothesis that CaSR is the source of the NIR autofluorescence peak seen at 822 nm. The relative intensities of the fluorescence emission seen in the colon and kidney tissues are also in agreement with the CaSR hypothesis. CaSR expression in the epithelial lining of the colon is relatively low in comparison to kidney, where it is expressed throughout the renal tubule and particularly high levels in the cortical thick ascending limb of the nephron. In combination with the pathological data, these findings further strengthen the argument that NIR emission originates from some feature within the CaSR. In addition, the findings suggest NIR autofluorescence can be utilized to investigate CaSR mediated pathology in the kidney and colon, as well as other tissues where it is expressed, such as the bone. In fact, the clinical data acquired from thyroid and hyperparathyroid disease, along with the *in vitro* data acquired from Wilm's tumor specimens contributes to the evidence that CaSR is in fact responsible for fluorescence emission at 822 nm.

Future studies

To characterize and further validate CaSR as the fluorophore responsible for the signal generated in the parathyroid gland, we propose that a number of protocols are carried out. Investigating the optical properties and EEM measurements of tissues and disease models known to express or alter the expression of CaSR, including kidney,

colon, brain, prostate cancer, breast cancer, and Wilms' tumor may shed light on the signal source. Comparison of CaSR transfected and wild-type HEK-293 cells will give a controlled model to assess the impact of the presence of CaSR on generation of autofluorescence signal and will yield valuable information. As multiple antibodies are available for CaSR assays, repeating the previous studies for the disease and normal tissue models may should clarify the impact of CaSR regulation and concentrations on the generated fluorescence. Finally, analysis of the inherent bond structure and bandgap energies for CaSR may explain its inherent ability to generate the fluorescence detected in numerous tissues, and provide further information to optimize excitation for future applications.

References

1. L. Sherwood, "Human physiology: from cells to systems" Brooks Cole; (7^{th} Edition) (2009).
2. G. Doherty, "Thyroid and Parathyorid," in Oncology: an evidence-based approach (A. E. Chang, P. A. Ganz, D. F. Hayes, T. Kinsella, H. I. Pass, J. H. Schiller, R. M. Stone, V. Strecher – Editors), Springer, (1^{st} Edition) (2006).
3. J. K. Harness, J. A. van Heerden, S. Lennquist, M. Rothmund, B. H. Barraclough, A. W. Goode, I. B. Rosen, Y. Fujimoto and C. Proye, "Future of thyroid surgery and training surgeons to meet the expectations of 2000 and beyond," World J Surg 24(8), 976-982 (2000)

4. S. Ozbas, S. Kocak, S. Aydintug, A. Cakmak, M. A. Demirkiran and G. C. Wishart, "Comparison of the complications of subtotal, near total and total thyroidectomy in the surgical management of multinodular goitre," Endocrine journal 52(2), 199-205 (2005)

5. T. Reeve and N. W. Thompson, "Complications of thyroid surgery: how to avoid them, how to manage them, and observations on their possible effect on the whole patient," World J Surg 24(8), 971-975 (2000)

6. C. Paras, M. Keller, L. White, J. Phay and A. Mahadevan-Jansen, "Near-infrared autofluorescence for the detection of parathyroid glands," J Biomed Opt 16(6), 067012 (2011)

7. J. R. Lakowicz, "Introduction to Fluorescence," in Principles of Fluorescence Spectroscopy, pp. 1-26, Springer (3rd Edition), (2006).

8. Z. Huang, H. Lui, X. K. Chen, A. Alajlan, D. I. McLean and H. Zeng, "Raman spectroscopy of in vivo cutaneous melanin," J Biomed Opt 9(6), 1198-1205 (2004)

9. A. Mahadevan-Jansen, M. F. Mitchell, N. Ramanujam, U. Utzinger and R. Richards-Kortum, "Development of a fiber optic probe to measure NIR Raman spectra of cervical tissue in vivo," Photochemistry and photobiology 68(3), 427-431 (1998)

10. E. Berber, R. T. Parikh, N. Ballem, C. N. Garner, M. Milas and A. E. Siperstein, "Factors contributing to negative parathyroid localization: an analysis of 1000 patients," Surgery 144(1), 74-79 (2008)

11. D. L. Fraker, H. Harsono and R. Lewis, "Minimally invasive parathyroidectomy: benefits and requirements of localization, diagnosis, and intraoperative PTH monitoring. long-term results," World J Surg 33(11), 2256-2265 (2009)

12. O. Hessman, P. Stalberg, A. Sundin, U. Garske, C. Rudberg, L. G. Eriksson, P. Hellman and G. Akerstrom, "High success rate of parathyroid reoperation may be achieved with improved localization diagnosis," World J Surg 32(5), 774-781; discussion 782-773 (2008)

13. A. Komisar, "Parathyroid localization," Operative Techniques in Otolaryngology-Head and Neck Surgery 13(3), 219-222 (2002)

14. J. I. Lew and C. C. Solorzano, "Surgical management of primary hyperparathyroidism: state of the art," Surg Clin North Am 89(5), 1205-1225 (2009)

15. R. Prommegger, G. Wimmer, C. Profanter, T. Sauper, M. Sieb, P. Kovacs, R. Bale, D. Putzer, M. Gabriel and R. Margreiter, "Virtual neck exploration: a new method for localizing abnormal parathyroid glands," Ann Surg 250(5), 761-765 (2009)

16. S. B. Reeder, T. S. Desser, R. J. Weigel and R. B. Jeffrey, "Sonography in primary hyperparathyroidism: review with emphasis on scanning technique," J Ultrasound Med, 21(5), 539-552; quiz 553-534 (2002)

17. M. E. Spieth, J. Gough and D. L. Kasner, "Role of US with supplemental CT for localization of parathyroid adenomas," Radiology 223(3), 878-879; author reply 879 (2002)

18. M. E. Tublin, D. A. Pryma, J. H. Yim, J. B. Ogilvie, J. M. Mountz, B. Bencherif and S. E. Carty, "Localization of parathyroid adenomas by sonography and technetium tc 99m sestamibi single-photon emission computed tomography before minimally invasive parathyroidectomy: are both studies really needed?," J Ultrasound Med, 28(2), 183-190 (2009)

19. L. Knudsen, C. K. Johansson, P. A. Philipsen, M. Gniadecka and H. C. Wulf, "Natural variations and reproducibility of in vivo near-infrared Fourier transform Raman spectroscopy of normal human skin," J Raman Spectrosc 33(7), 574-579 (2002)

20. E. Vargis, T. Byrd, Q. Logan, D. Khabele and A. Mahadevan-Jansen, "Sensitivity of Raman spectroscopy to normal patient variability," J Biomed Opt 16(11), 117004 (2011)

21. S. A. Prahl, M. J. van Gemert and A. J. Welch, "Determining the optical properties of turbid mediaby using the adding-doubling method," Appl Opt 32(4), 559-568 (1993)

22. N. Chattopadhyay and E. M. Brown, "Cellular "sensing" of extracellular calcium (Ca(2+)(o)): emerging roles in regulating diverse physiological functions," Cellular signalling 12(6), 361-366 (2000)

23. E. M. Brown, G. Gamba, D. Riccardi, M. Lombardi, R. Butters, O. Kifor, A. Sun, M. A. Hediger, J. Lytton and S. C. Hebert, "Cloning and characterization of an extracellular Ca(2+)-sensing receptor from bovine parathyroid," Nature 366(6455), 575-580 (1993)

24. L. D'Souza-Li, "The calcium-sensing receptor and related diseases," Arquivos brasileiros de endocrinologia e metabologia 50(4), 628-639 (2006)

25. D. Goltzman, "Hormone Secretion," in Principles and practice of endocrinology and metabolism (K. L. Becker – Editor), pp. xxxiv, 2477 p., Lippincott Williams and Wilkins, (2001).

26. E. M. Brown, "Hormonal Control of Calcium Homeostasis," in Principles and Practice of Endocrinology & Metabolism (K. L. Becker - Editor), p. 482, Lippincott Williams & Wilkins, (2001).

27. O. Kifor, F. D. Moore, Jr., P. Wang, M. Goldstein, P. Vassilev, I. Kifor, S. C. Hebert and E. M. Brown, "Reduced immunostaining for the extracellular Ca2+-sensing receptor in primary and uremic secondary hyperparathyroidism," J Clin Endocrinol Metab 81(4), 1598-1606 (1996)

28. A. Kienle and T. Glanzmann, "In vivo determination of the optical properties of muscle with time-resolved reflectance using a layered model," Phys Med Biol 44(11), 2689-2702 (1999)

CHAPTER V

Development of a Real-time Intra-operative Parathyroid Visualization System for Endocrine Surgery

Constantine Paras,[1] Isaac Pence, [1] and Anita Mahadevan-Jansen[1,4]

[1]*Department of Biomedical Engineering, Vanderbilt University, Nashville, TN 37235, USA*

[4]*Department of Neurological Surgery, Vanderbilt University, Nashville, TN 37235, USA*

[*]*Corresponding author: anita.mahadevan-jansen@vanderbilt.edu*

Introduction

The current intra-operative method for identifying parathyroid glands involves a systematic exploration of the neck in which the surgeon is primarily relying on visual distinction to identify target tissues. The complications that arise due to this method have an incidence that is directly proportional to the extent of thyroid tissue removed and inversely proportional to the experience of the operating surgeon (1). Other existing limitations of this process are the duration of the surgery, the exploratory nature of the procedure, and the difficulty in correlating preoperative images with real-time exploration of the anatomy. The preoperative technique, Sestamibi scintigraphy has a reported sensitivity varying widely from 43-100% and has proven to be the best initial preoperative modality for locating hyper-functioning parathyroid tissue (2). This method yields no precise location for parathyroid glands, no way of knowing if all of a gland has been removed during surgery, and no context for the other parathyroid glands that must be preserved during the course of the operation. In fact, current standards rely on histopathology or the post-operative diagnosis of symptoms to determine if the parathyroid glands have been accidentally or incompletely removed during a procedure (3). Therefore, the development of an accurate, automated diagnostic method could allow faster, more effective patient management (4, 5).

Optical spectroscopy has been demonstrated as a technique to accurately detect differences in tissue architecture and biochemical composition in a fast and non-invasive fashion. In particular, the use of fluorescence spectroscopy has been of great interest in the development of clinical diagnostic tools. Measurements of human tissues can be made *in situ* in real-time without the need for tissue preparation, and subsequent

diagnosis could potentially be automated with the creation of a robust algorithm based on tissue fluorescence properties (6). The intrinsic fluorescence of some tissue, known as autofluorescence, is typically exhibited in the range of ultraviolet and visible wavelengths of light, 400-700nm, but is generally more common at the lower excitation wavelengths (7). Early studies have demonstrated the difference in autofluorescence intensity of the parathyroid and thyroid tissues using near infrared (NIR) light to excite the tissues in question (Chapter 3). Specifically, the intensity of the parathyroid gland autofluorescence has consistently been shown to be between 2-35 times greater than the autofluorescence of the thyroid gland and even higher for other tissues in the vicinity including adipose, lymph, muscle, and nerve tissue. The ongoing study uses a fiber-optic probe-based fluorescence spectrograph and 785 nm excitation source and has shown promise in distinguishing between parathyroid and thyroid tissue in real-time measurements of approximately 300 ms. This detection system is capable of providing information to the surgeon that would otherwise not be available for help in distinguishing between these visually similar tissues.

Despite the aid provided by this new technique, this probe-based system has several limitations to its direct clinical translation and implementation. The nature of probe-based measurements yields only localized information about tissues for the surgeon. Therefore, there is no spatial context available during the surgery without time-prohibitive measurements of the entire region of interest. The system requires that the surgeon pause during the surgery to hold the fiber-optic probe, both interfering with other instruments that are important and consuming time that could otherwise be used during the procedure. This fiber optic probe based spectrograph system may also be cost-prohibitive for general

surgeons due to the expenses associated with purchasing a fluorescence spectrograph and processing system with an approximate value of $12,000.

To circumvent these limitations, an imaging solution is proposed in which the surgeon could obtain a spatial context for the tissues in question in a real-time manner. Because the autofluorescence signal emits at approximately 822 nm, most low-cost CCD cameras are not capable of detecting the light with the necessary efficiency. In order to demonstrate the potential of this method, a proof-of-concept test was performed using the Princeton Instruments PhotonMax 512 spectral imaging camera attached to a surgical microscope for detection of the light. The sample tissues, *ex vivo* thyroid and parathyroid glands, were illuminated with an unfocused beam using a laser power of 80mW at the fiber tip. The system and procedure utilized during this demonstration, depicted in Figure 1, yielded promising results which led to further investigation of potential solutions. Figure 2 shown the resulting image obtained where the brighter signal is obtained from the parathyroid tissue as compared the less intense thyroid gland. The spectral imaging camera is optimized for the detection of NIR wavelengths with the necessary high quantum efficiency and successfully demonstrated feasibility of optical detection of the relative higher intensity of the parathyroid gland. Major drawbacks to this system, however, includes the size of

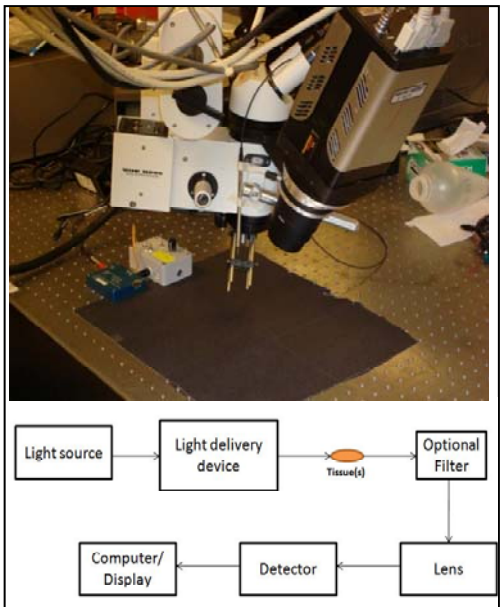

Figure 1: *Top: Image of spectral imaging camera for proof-of-concept. Bottom: Flowchart schematic of imaging system components.*

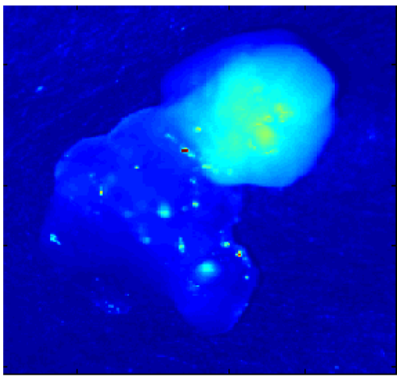

Figure 2: *NIR image of thyroid (left) and parathyroid (right) tissue placed adjacent to each other in a petridish.*

the system, which employs a large surgical microscope, the timely post-acquisition processing of the images to clearly distinguish the tissues in question, and the cost of the system, approximately $30,000 for the spectral imaging camera alone. This cost is potentially the most daunting limitation to the clinical translation of the system into use in surgical suites, and thus the investigation of a low-cost alternative began.

Here, an alternative to the spectral imaging camera using a commercial NIR viewer is presented. FJW Optical's Find-R-Scope© is a relatively low cost commercial NIR viewer that is intended for applications ranging from laser system alignment to viewing art and historical documents (8). The proposed system is intended to allow the surgeon to visualize the different tissues and borders in the field of view based upon the observed tissue fluorescent intensity. Other surgical considerations were addressed in a limited fashion, including integration with existing technology into the surgical suite. The system design described in this paper would improve the design of the IR viewer to integrate the system into a surgical suite with existing equipment. The system developed would also yield information not available via other technology based techniques, be informative and easy to use, requiring little or no training. It should operate in real-time with little user interaction and provide intuitive feedback to the surgeon. The system should also serve to reduce the time and error-rate associated with current surgical procedures, hopefully eliminating the need for costly reoperative cases.

Focusing on some considerations provided by Dr. Phay and Dr. Broome of the Vanderbilt Endocrine Surgery Center, the outcome of the design process needed first and foremost, to be useful to the surgeons. This would be best accomplished by providing visual feedback and imaging data, giving morphological and spatial context to the tissues of interest. The system must not interfere with the surgical procedure. One proposed method was to develop a head-mounted device based upon CMOS technology. This method was abandoned due to the inherent drawbacks of current standard of image intensifier technology, which allows the visualization of the NIR autofluorescence that this method employs. Not only are third and fourth generation image intensifiers cost-prohibitive, but they lack the needed sensitivity in the spectral region for which this application is intended. To address this, the older, reliable photomultiplier tube (PMT) based device was selected as a low-cost alternative. This option would allow the images captured to be displayed on the video screens in the surgical suite that the surgeons are familiar with. A subsequent design constraint followed form the necessity of obtaining these images while remaining outside the sterile halo, a 3 foot diameter space surrounding the patient in surgery. This constraint directly led to the need for improved optics for the necessary resolution at three feet as well as the ability to focus on ranges from the surgical incision of about 6 inches to the margins of the parathyroid gland itself of at least 2mm. In order to address these needs, the design process was undertaken to produce a system that would provide real-time feedback in distinction of these tissues for the surgeons benefit.

Methods and Materials

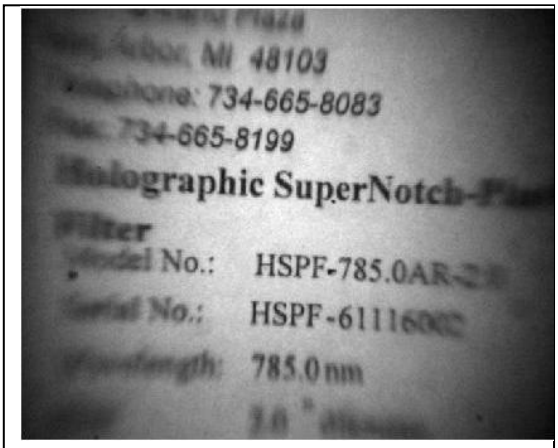

Figure 3: *An image of a Kaiser© filter product label demonstrating spherical aberrations of imaging system.*

Several limitations existed within the inherited system that required attention prior to consideration for translation into a clinical or surgical setting. The most notable of these was the limiting inadequacy of optical components within the commercial viewer. This device had internal parts that were necessary to the functioning of the system, detecting wavelengths from 350-1350 nm and with a peak sensitivity reported at 800nm, but other system components required attention. The first major concern faced was the presence of spherical aberration in the imaging system. This distortion that appears radially from the center of the lens allowed for precise resolution at the center of the images but the edges remained out of focus, as seen in Figure 3. For the developed system to be clinically useful, the entire field of view must be undistorted to give the surgeon maximum information regarding the area of interest. As this distortion was the result of both the PMT and the low-quality lens in combination, the lens configuration was investigated. Along with the image distortion, the viewer lacked magnification and was incapable of providing the requisite focus for imaging the field of view with the needed resolution. The minimal resolution was determined to be higher than the size reported for parathyroid gland dimensions, requiring the system be capable of resolving structures smaller than 1-2 mm. Attaining this resolution from outside the sterile halo of three feet and incorporating the design into the surgical suite led to the

redesign of the body of the IR viewer, to allow mounting of the system to an arm over the patient, clear of the surgeon and sterile halo. In addition, an adapter was designed such that the attachment of standard c-mount lenses could be introduced in place of the proprietary lens mount that the viewer originally had. These plans were carried out by the Vanderbilt Physics machine shop. As seen in figure 4, the viewer was altered from a handheld device to one intended for mounting with an improved lens.

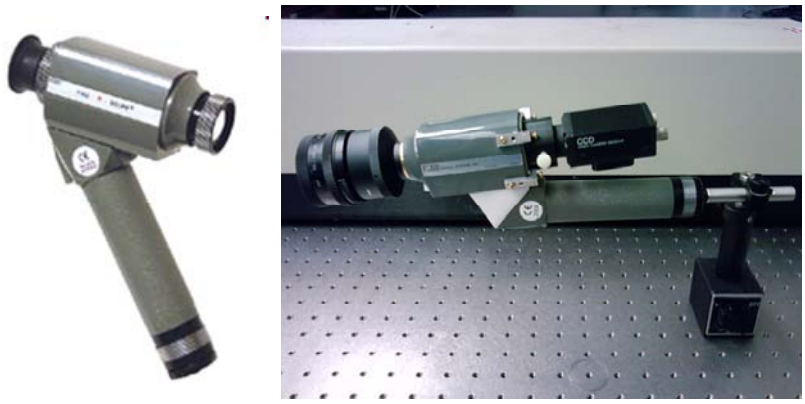

(a) (b)

Figure 4: *(a) Original commercial Find-R-Scope intended for handheld use. (b) Modified IR viewer mounted with a c-mount adapter and lens*

To test this design, an initial spatial resolution test was performed using a NBS 1963A resolution test card for the original lens, a potential replacement c-mount lens (Navitar 7000) and for the CCD directly coupled to the Navitar lens as a benchmark for optimal performance. These images were collected with a separation of the lens and target card of three feet, using a diffuse reflectance standard (Spectralon© from Labshpere, Inc.) as a background illuminated by a halogen lamp. The overhead room lights, both fluorescent and incandescent were shut off so that the only illumination detected was that of the target. Images were collected at the maximum magnification for the lenses in question, sequentially focusing on line pairs of increasing resolution. The

collected images were then analyzed using Matlab to determine the existing limits of resolution.

As the needed resolutions were not met with this configuration, the design for the lens adapter was revisited and found to be insufficient for coupling the c-mount lens to the

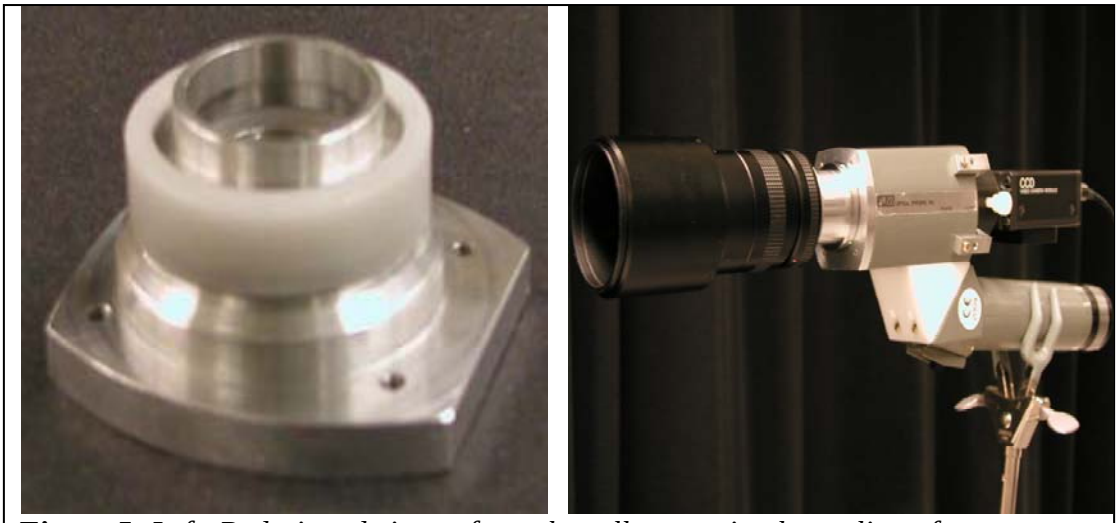

Figure 5: *Left: Redesigned viewer front that allows optimal coupling of c-mount lenses. Right: The assembled IR viewer and CCD system.*

PMT acceptance region. By disassembling the IR viewer body and designing a new front end attachment to account for the appropriate image distance for c-mount lenses into the acceptance field of the PMT, a new interface was developed to accomplish multiple goals. These requirements were 1) the attachment of the desired c-mount lens to the viewer, and 2) the inclusion of a filter to remove the strong signal of the laser excitation wavelength. This redesign was completed and subsequent spatial resolution tests were carried out under the same conditions as previously described for both the Navitar 7000 and Nikon 50mm lenses, with the exception that a 1951 USAF resolution target was used in place of the 1963 NBS target card. The new front end and assembled viewer can be seen in figure 5.

With the desired performance for the distance at three feet, other issues were subsequently addressed. In order to block the excitation light from the laser source that was saturating the field of view, several filters were tested resulting in the inclusion of a Semrock RazorEdge filter© in the beam path for consistent rejection of the excitation light. As this filter offers excitation rejection via 808nm long pass filter function, it was also necessary to investigate methods for co-registration that would allow the surgeon to distinguish where in the field he or she is operating. Rather than incorporating a second camera, the use of another NIR light source, an LED, was adopted such that the intensity would not saturate the detector and the filter would not block the NIR wavelengths that the PMT was capable of detecting.

For the display and processing, a VI was created using LabView 8.5 with an IMAQ card that would allow images to be collected in real-time and displayed on any computer monitor. The developed instrument integrates a MATLAB node that is capable of speckle reduction, reduction of spherical aberration, and application of false color in a limited capacity. The spherical aberration program is based on work performed by Dr. Mark Mackanos which was originally intended to address aberrations associated with endoscopic cameras used in surgery. Likewise the application of false color is limited by the wide range of inter-patient variation in fluorescence levels. Further investigation is required as this variation must be accounted for, but possibilities for this will be address later on. The interface also allows the user to capture still frame images from the camera for later analysis or record keeping applications.

In order for this system to operate successfully, light from the laser must reach the tissues in question. Therefore, the calculated excitation irradiance was determined as a function of the separation between the light delivery method and the detector. This was undertaken to determine if the use of the Newport Liquid Light Guide was merited or if delivery through an Ocean Optics fiber optic cable was more appropriate, as demonstrated in Figure 6. This light guide was originally purchased to create a method of illuminating the entire sample region of tissue with sufficient power from the laser. Collected data and calculations from theoretical models of the behavior of the light from each of these delivery methods were found. This data was collected by translating a power meter in one dimension, incrementally measuring the maximum incident power at a given distance. While this is not irradiance by definition, the ray approximation and Gaussian approximation for light were used to determine a theory-based calculated irradiance at which the system was capable of delivering the energy necessary for excitation as defined by the conventions adopted by the probe-based fluorescence detection study.

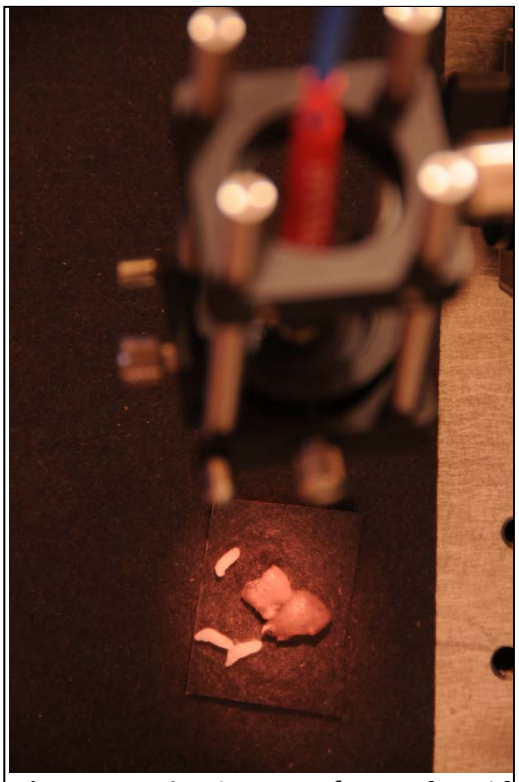

Figure 6: *An image of parathyroid and thyroid glandular tissue on matting under illumination by 785nm excitation light along with three grains of rice for comparison*

The limits of detection for the system also needed testing, which was quantified as the signal to noise ratio of the system as a function of irradiance. The IR viewer was focused

onto black matting that had been determined to have no reflectance or fluorescence signal using the probe-based system. Using the Ocean Optics fiber optic cable, and with the room lights turned off, the fiber tip was mounted perpendicular to the surface of the matting at a measured height. The power from the laser source was then measured at the fiber tip and used to calculate irradiance at the matting. The viewer was used to image the spot produced by the laser light at 785 nm from 3 feet away. For the purposes of this measurement, the signal was defined as the total number of counts in a standard region of interest at a calculated irradiance. The noise was calculated as the standard deviation of the region of interest with the laser turned off. These measurements were acquired at near threshold levels for visual distinction of the laser light. This determination was made for 785 nm light which is not exactly what is expected for 822 nm light, but based upon the response of the IR viewer, no significant differences are expected.

The final validation for the system was to combine all the various, individual parts into a functioning whole. The ability of the system to detect the differential autofluorescence of tissue was validated with *ex vivo* tissue samples that had been resected by the Endocrine Surgery Center. Using tissues that had been frozen at -80°C after excision, the system was setup with design characteristics in mind. The viewer was mounted three feet above the sample location and connected to the LabView interface for data collection. The laser source, fiber optic delivery, and NIR LED light were oriented such that they would illuminate the tissue samples simultaneously. The samples were removed from the freezer, rinsed and allowed to thaw in a saline bath. The tissue surface was then dried and placed on the non-fluorescent black matting to reduce image artifacts,

as seen in Figure 6. With the room lights off, images where acquired with the LabView software to capture the differential autofluorescence intensity of the tissues.

Results

Following each alteration made to the IR viewer, the spatial resolution was tested for a three foot separation between lens and target card. This was the initial criterion considered as to whether or not a design might be feasible. The previously reported resolution was 0.71mm at a separation distance of 4 inches. After the initial alteration, the original viewer lens remained unchanged. With a 3 foot separation, the lens was not capable of distinguishing any of the line pairs on the target. With the adapter in place, the maximum resolution attainable 0.91mm, but the images at this resolution were blurry and not unfit for a surgical imaging system. Upon completion of the re-designed front end, the Nikon 50mm fixed zoom lens afforded clarity and depth of field but the resolution maximum was 1.12 mm. The Navitar 7000 lens, however, allowed variable zoom to encompass the entire surgical field as well as the resolution to focus on the tissues from three feet away. The final calculated system spatial resolution is 0.28mm and the target can be seen in figure 7. This resolution is sufficient to vary the field of focus but still retain the spatial features that are necessary for the surgeon to perform the operation. One consideration that follows for the

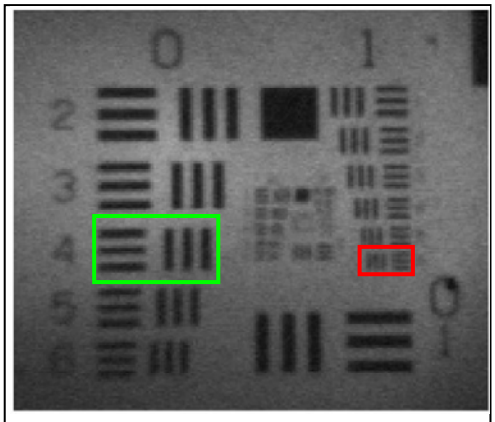

Figure 7: *Resolution target under NIR illumination, boxes correspond to previous (green) and current (red) resolutions.*

system to be clinically translated requires that the lens casing must be covered with a sterile drape in surgery to allow the surgeon or an assistant to reach up, position the viewer and adjust the zoom to the appropriate level without contaminating the sterile field.

The excitation irradiance as a function of the separation between the delivery mode and the sample is given in figure 8. The importance of this result is less quantitative in nature: primarily, this test excluded the Liquid Light Guide (LLG) from consideration as a design component as it was incapable of delivering the desired irradiance to the sample and back to the detector at distances comparable to the fiber optic alone. For the ray approximation, the fiber is the better option, but the underlying assumptions make it more likely that the Gaussian approximation is accurate, especially at distances greater than 3 times the core of the delivery device. For this more accurate approximation, both devices are predicted to give equal irradiance for approximately 87% of the light out of the medium, but because the LLG has a larger numerical aperture and is functioning in air, the irradiance is expected to diminish faster in this model than with the fiber.

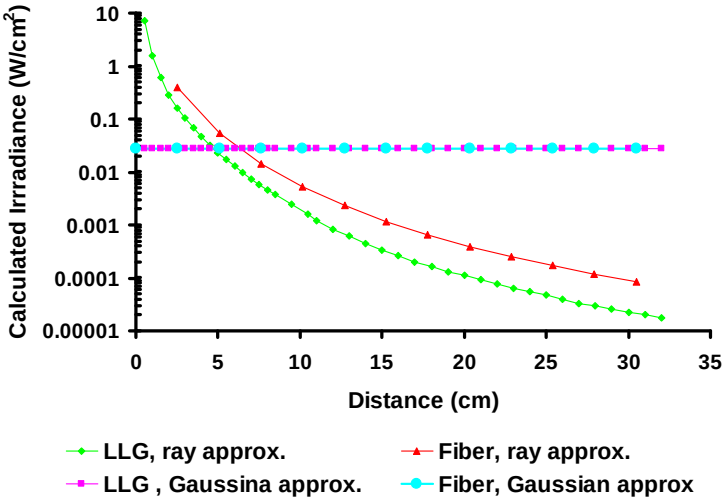

Figure 8: *The plot of calculated irradiance as a function of separation for the system excitation optimization.*

The calculated SNR for the system operating at 3 feet for 785nm light is shown in figure 9. Because the behavior of the PMT, which is responsible for the image conversion from NIR to visible wavelengths, is not considered to be linear in response, it is not possible to determine a threshold sensitivity for the system based on this data. This result does, however, explain that the irradiance associated with the minimum current at which the laser can operate with stability has a signal to noise ratio of over 100dB. The system is considered to be sensitive enough to detect the autofluorescence signal even from weak sources like the tissues. One caveat to this data is that the intensities collected here were all at 785nm. To truly characterize the response of the system, and excitation-emission matrix should be constructed, filtering a band of emission spectra and collecting values as a function of excitation wavelength. Finally the last validation method was to detect the differential autofluorescent signal from tissue samples *ex vivo*. Images of this result can be seen in figure 10. The intensity difference is visible even without application of the heat map.

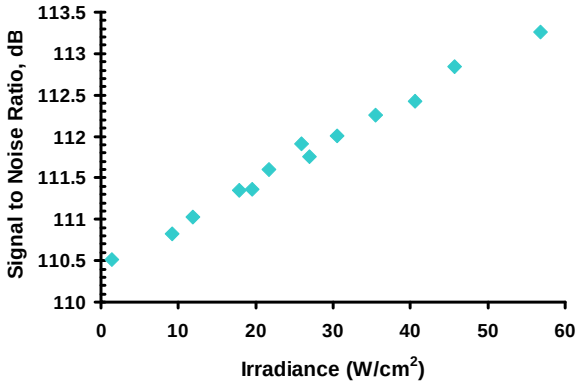

Figure 9: *System SNR from 3 feet as a function of laser irradiance.*

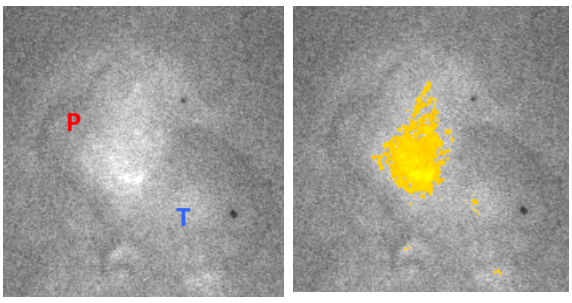

Figure 10: *Image of parathyroid and thyroid detected from 3 feet Right: Same image with overlay of fluorescent heat map to visualize tissue autofluorescence.*

This image and others like it yield a final validation to the success of this method in providing a method of

differentiating the visually similar parathyroid and thyroid gland tissues *ex vivo*. To ensure that the observed signal was not specular reflectance of the excitation source that was improperly filtered, images were collected from the samples at 90º angles, during which the observed signal was maintained. This conservation of observed signal suggests that autofluorescence is imaged as the reflectance would change with angle.

An economic analysis of the project was completed to determine the incurred costs and benefits of such a system, comparing the total system cost with the cost associated with current values for a minimally-invasive parathyroidectomy. The underlying assumption is that the cost of complications is the cost of a repeat surgery. This analysis also neglects other endocrine surgery cases that could result in inadvertent parathyroid damage or removal.

System Cost	
Modfied IR Viewer	$1,990
Sony CCD camera	$480
Nazvitar 7000 lens	$460
Semrock © filter	$420
Ocean Optics© fiber	$115
Total cost	$3,465

The cost of a single parathyroidectomy has been reported as $4986 (9). Assuming that a hospital performs 50 of these procedures a year, that the failure rate of the procedure is 5%, and that this system is capable of resolving complications, then the annual savings by the hospital after purchasing the system is $9000. This assumption is that all cases of parathyroidectomy will be successfully handled by the use of this system which is optimistic, but also ignores other endocrine surgical procedure that might benefit from the use of this system. This also does not account for legal fees that would be reduced as well as the values associated with an improved quality of life after surgery.

Conclusions

The primary goal of this project was to develop a system that was capable of detecting the autofluorescent difference between parathyroid and thyroid tissues while fulfilling the requirements for integration into the surgical setting. Successful demonstration of these requirements has been carried out to some extent, taking into consideration the opinions of the surgeons consulted. The secondary goal of this design was to arrive at the system in a way that the price of the entire system would allow for reproduction and clinical translation even to small hospitals that would be most in need of a device of this type. In comparison to the previously mentioned Princeton Instruments PhotonMax spectral imaging camera alone, this entire system, not including the 785nm diode laser and the computer and LabView programming suite, is less than 12% of the cost. Another metric by which the system has yet to be verified is the actual time reduced in surgery through the use of the imaging system. Overall the design is successful in delivering the desired real-time feedback that affords a spatial context to the fluorescence information of the tissues examined. The system has a resolution that is now higher at 3 feet than previously attained at 4 inches. The system has also made the initial steps in implementing algorithms to improve the images displayed on the surgical monitors so that there are no artifacts introduced by the system. Continuing forward, this project should address the few limitations with which it is faced, but holistically could soon be implemented in endocrine and general surgical suites to improve outcomes and quality of life.

Recommendations

Some limitations to this design do exist and may need to be addressed in the future. One primary focus should be the investigation of a different method of capturing the NIR signal other than PMT. As a PMT ages, it develops black spots on its screen that are no longer able to transduce NIR to visible light, limiting its usefulness in providing images and contrast between intensities. While this may need to be addressed, it is unlikely that a better alternative will be found at a comparable price. Another limitation is the current implementation of the programming interface. Currently, the MATLAB algorithm that is used for correction of aberrations requires about one second to process images and remove distortion, a process that would limit the real-time data acquisition. It is therefore necessary to determine if this system experiences enough distortion from these aberrations to merit the use of such a program and if so to develop a similar algorithm in a faster C-based language.

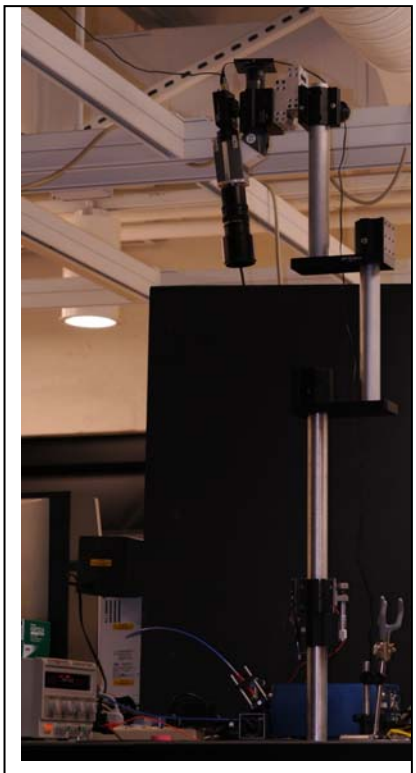

Figure 11: *Picture of entire system, with IR viewer mounted outside the 3 foot halo.*

The implementation of false color and heat mapping to distinguish fluorescence levels is also a factor that needs to be addressed. Because there is significant variability between patient fluorescence levels, as corroborated through the probe-based study, there is a need for a fluorescent standard that will retain constant intensity over time with

which the system can be calibrated and checked for variation over its operational lifetime. The use of soluble dyes, fluorescent microspheres, or even other intensity standards has been difficult to justify as most do not function in this spectral region, so further investigation is necessary.

An optimal method for incorporating this system into the surgical suite is needed, requiring some mounting device for the viewer as well as an improved method of exciting the tissues that does not require the current proximity to the patient. As seen in figure 11, the current configuration is optimized for mounting, but may not be as easily integrated into the surgical suite as necessary for regular use. This investigation may lead to expanded translatability of the device if the excitation light can be drawn further away from the patient.

Finally, more samples need to be collected and the development of a discrimination algorithm should be undertaken such that the system could potentially identify benign and healthy parathyroid and thyroid tissues and remove the surgeon's bias in finding glands based on subjective anatomical markers.

References

1. A. R. Shaha and B. M. Jaffe, "Parathyroid preservation during thyroid surgery," American journal of otolaryngology 19(2), 113-117 (1998)

2. S. R. Anderson, A. Vaughn, D. Karakla and J. T. Wadsworth, "Effectiveness of surgeon interpretation of technetium tc 99m sestamibi scans in localizing parathyroid adenomas," Arch Otolaryngol Head Neck Surg 134(9), 953-957 (2008)

3. A. Frilling and F. Weber, "Complications in Thyroid and Parathyroid Surgery," in Surgery of the Thyroid and Parathyroid Glands, pp. 217-224 (2007).

4. A. T. Ahuja, K. T. Wong, A. S. Ching, M. K. Fung, J. Y. Lau, E. H. Yuen and A. D. King, "Imaging for primary hyperparathyroidism--what beginners should know," Clin Radiol 59(11), 967-976 (2004)

5. S. Fakhran, B. F. t. Branstetter and D. A. Pryma, "Parathyroid imaging," Neuroimaging Clin N Am 18(3), 537-549, ix (2008)

6. N. Ramanujam, M. F. Mitchell, A. Mahadevan, S. Thomsen, A. Malpica, T. Wright, N. Atkinson and R. Richards-Kortum, "Spectroscopic diagnosis of cervical intraepithelial neoplasia (CIN) in vivo using laser-induced fluorescence spectra at multiple excitation wavelengths," Lasers Surg Med 19(1), 63-74 (1996)

7. J. R. Lakowicz, "Fluorophores," in Principles of Fluorescence Spectroscopy, pp. 63-95, Springer (3rd Edition), (2006).

8. FJW Optical Systems, http://www.findrscope.com/ (2012).

9. K. Zanocco, P. Angelos and C. Sturgeon, "Cost-effectiveness analysis of parathyroidectomy for asymptomatic primary hyperparathyroidism," Surgery 140(6), 874-881; discussion 881-872 (2006)

Chapter VI

Conclusions

Constantine Paras,[1,*] and Anita Mahadevan-Jansen[1,]

[1]*Department of Biomedical Engineering, Vanderbilt University, Nashville, TN 37235, USA*

[*]*Corresponding author: anita.mahadevan-jansen@vanderbilt.edu*

Summary of Chapters

Thyroidectomy is a commonly performed surgical procedure for the treatment of thyroid disease. Parathyroidectomy involves a similar procedure performed for treating parathyroid disease. Such endocrine surgeries traditionally require meticulous dissection and resection of diseased glands while leaving the normal glands intact, guided only by visual recognition. Inadvertent removal of parathyroid glands is a recognized complication of this procedure. The incidence of inadvertent parathyroidectomy ranges from 8% to 19% out of patients undergoing total thyroidectomy (Sakorafas 2005). Such inadvertent removal or accidental injury of the parathyroid may lead to complications such as postoperative hypocalcemia and hypoparathyroidism that could have consequences on the longterm regulation of calcium homeostasis post-operatively.

Thus there is a critical need for a diagnostic tool that provides sensitive real-time detection of parathyroid glands during thyroidectomies and parathyroidectomies. This method should be highly effective at differentiating thyroid and parathyroid glands from each of other as well as the other tissues in the region thereby avoiding accidental injury or removal of the paraythyroid glands. *This dissertation seeks to prove the hypothesis that intrinsic near-infrared fluorescence can provide sensitive, real-time identification of parathyroid tissues as compared to thyroid and other tissues to guide dissection and resection during surgery.* The main objective of this project then was to develop a technique based on near- infrared (NIR) autofluorescence that enables intra-operative detection of parathyroid glands such that accidental removal is minimized by supplementing the standards of visual inspection. Since current procedures are guided solely by visual inspection, this proposal presents a novel automated method of surgical

guidance that can minimize surgical error and improve patient outcome. The broader scope of this project is to provide real-time spectroscopic images of the tissues in the neck with automated differentiation and high sensitivity that can be used to anatomically guide surgeons during thyroidectomies and parathyroidectomies.

This dissertation consists of three manuscripts that outline this research towards the development of near infrared spectroscopy and imaging for the anatomical detection of the parathyroid gland in vivo to guide endocrine surgery. The three specific aims described in this document not only prove the stated hypothesis but also help in developing an understanding of the scientific basis for the success of the technique. The results of this work will have a significant impact on health care by providing guidance towards dissection and resection of thyroid and parathyroid tissues. This would potentially result in fewer complications due to accidental injury or incomplete removal of parathyroid tissue.

Each specific aim addressed in each of chapters 3, 4 and 5 describe the experimentation and analysis that leads to the proposed endpoint. Specifically, in chapter 3 a pilot in vivo study was conducted to assess the ability of NIR fluorescence to identify parathyroid glands during thyroid and parathyroidectomies. Fluorescence measurements at 785 nm excitation were obtained intra-operatively from the different tissues exposed in the neck region in 21 patients undergoing endocrine surgery. The fluorescence intensity of the parathyroid gland was found to be consistently greater than that of the thyroid and all other tissues in the neck of all patients. In particular, parathyroid fluorescence was 2-35 times higher than that of the thyroid tissues with peak fluorescence occurring at 822

nm. These results indicate that NIR fluorescence has the potential to be an excellent optical tool to locate parathyroid tissue during surgery

In chapter 4, the fluorescence and optical properties of parathyroid and thyroid tissues were analyzed to obtain a better understanding of the behavior of these tissues and to arrive at a hypothesis for the basis of the observed high fluorescence. Based on these results, a hypothesis was derive whereby calcium sensing receptors (CaSR) was identified as the potential fluorophore in these tissues that yields a consistently high near infrared fluorescence. Preliminary analysis was performed on other tissues known to have CaSR and was shown to also exhibit increased fluorescence at the level of that observed in the thyroid. Further, in a disease model of Wilm's tumor known to have compromised levels of CaSR, significantly reduced levels of this fluorescence was also observed attesting to the validity of the results described in Chapter 3.

In chapter 5, a practical design towards an imaging system was developed and tested in order to provide spatial as well as spectral information during the surgical procedure for realtime feedback. This system was successfully prototyped and tested in vitro and relevant hardware and software was designed.

Thus this dissertation successfully demonstrates the feasibility of applying near infrared fluorescence for the detection of parathyroid glands. The implications of this work extends to beyond the detection of the parathyroid tissue. The increased fluorescence allows for detection of metastatic tumor cells from these tissues that have migrated in to the lymph node without the the need for a lymph node resection. CaSR fluorescence also indicates that this technique can be used for the detection of conditions

where these receptors may be compromised such as Wilm's tumor of the kidney. This technique can also be used to improve our fundamental understanding of CaSR.

Future work

There are several steps that need to be taken to further the research initiated by this dissertation. Chapter 3 indicates that the parathyroid fluorescence varies between 2-35 times that of the thyroid. The variability of this observed *in vivo* fluorescence will need to be characterized in order to validate the accuracy of this technique. Potential sources of variability include gender, age, hormonal state etc. While Chapter 4 describes a preliminary basis for the hypothesis that CaSR is responsible for the near infrared fluorescence this hypothesis needs to be extensively validated through studies in wild-type and knock-out models of these receptors in cells and animal models. Immunohistochemistry and mass spectrometry analysis can be additionally used to obtain a better understanding of what in this molecule engenders this fluorescence so far in the near infrared – never before observed in biological tissues. Finally, a feasible design for an imaging device was developed in Chapter 5 and tested in vitro. This system needs to be tested in vivo and a method of registration of the images obtained needs to be developed. Other options for such a device also need to be considered for seamless integration into the operating room. . Finally a critical step in the implementation of this technology will be a large scale clinical trial under FDA approval that will robustly verify the results of this dissertation and take it to the patient.

Bibliography

1. J. Hubbard, W. B. Inabnet, C-Y. Lo, "Endcrine Surgery" (1st Edition), Springer, (2011).
2. Medicinenet, "Parathyroid Glands," p. Anatomy of neck region, http://www.medicinenet.com/parathyroidectomy/article.htm (2007)
3. R. D. Bliss, P. G. Gauger and L. W. Delbridge, "Surgeon's approach to the thyroid gland: surgical anatomy and the importance of technique," World J Surg 24(8), 891-897 (2000)
4. F. R. Miller, "Surgical anatomy of the thyroid and parathyroid glands," Otolaryngol Clin North Am 36(1), 1-7, vii (2003)
5. A. R. Shaha and B. M. Jaffe, "Parathyroid preservation during thyroid surgery," American journal of otolaryngology 19(2), 113-117 (1998)
6. H. N. Le and J. A. Norton, "Parathyroid," in Essential Practice of Surgery (J. A. Norton, R. R. Bollinger, A. E. Chang, S .F. Lowery, S. J. Mulvihill, H. I. Pass, R. W. Thompson – Editors), pp. 369-378, Springer (1st Edition), (2003).
7. A. H. Elgazzar, "Parathyroid Gland," in The Pathophysiologic Basis of Nuclear Medicine, (A. H. Elgazzar – Editor), pp. 222-237, Springer (2nd Edition), (2006).
8. I. R. McDougall, "Management of thyroid cancer and related nodular disease", Springer,)1st Edition), (2006).
9. S. Nussey, S. Whitehead, " Endocrinology", BIOS Scientific Publishers, (2001).

10. L. Kim, M. W. Krause, V. Kantorvich, "Hyperparathyroidism," (G. T. Griffing – Editor), http://emedicine.medscape.com/article/127351-overview , (2011).
11. J. A. Sosa, N. R. Powe, M. A. Levine, R. Udelsman and M. A. Zeiger, "Profile of a clinical practice: Thresholds for surgery and surgical outcomes for patients with primary hyperparathyroidism: a national survey of endocrine surgeons," J Clin Endocrinol Metab 83(8), 2658-2665 (1998)
12. D. Scott-Coombes, "The parathyroid glands: hyperparathyroidism and hypercalcaemia," Surgery (Oxford) 21(12), 309-312 (2003)
13. A. T. Ahuja, K. T. Wong, A. S. Ching, M. K. Fung, J. Y. Lau, E. H. Yuen and A. D. King, "Imaging for primary hyperparathyroidism--what beginners should know," Clin Radiol 59(11), 967-976 (2004)
14. ATA, "Thyroid Surgery," American Thyroid Association, http://www.thyroid.org/patients/brochures/ThyroidSurgery.pdf, (2005).
15. ACS, "Detailed Guide: Thyroid Cancer," American Cancer Society, http://www.cancer.org/Cancer/ThyroidCancer/DetailedGuide/index, (2008).
16. D. T. Lin, S. G. Patel, A. R. Shaha, B. Singh and J. P. Shah, "Incidence of inadvertent parathyroid removal during thyroidectomy," The Laryngoscope 112(4), 608-611 (2002)
17. F. Pattou, F. Combemale, S. Fabre, B. Carnaille, M. Decoulx, J. L. Wemeau, A. Racadot and C. Proye, "Hypocalcemia following thyroid surgery: incidence and prediction of outcome," World J Surg 22(7), 718-724 (1998)

18. A. Frilling and F. Weber, "Complications in Thyroid and Parathyroid Surgery," in Surgery of the Thyroid and Parathyroid Glands (D. Oertili, R. Udelsman – Editors), pp. 217-224, (1st Edition), (2007).

19. G. H. Sakorafas, V. Stafyla, C. Bramis, N. Kotsifopoulos, T. Kolettis and G. Kassaras, "Incidental parathyroidectomy during thyroid surgery: an underappreciated complication of thyroidectomy," World J Surg 29(12), 1539-1543 (2005)

20. R. L. Prosst, J. Gahlen, P. Schnuelle, S. Post and F. Willeke, "Fluorescence-guided minimally invasive parathyroidectomy: a novel surgical therapy for secondary hyperparathyroidism," Am J Kidney Dis 48(2), 327-331 (2006)

21. S. Fakhran, B. F. t. Branstetter and D. A. Pryma, "Parathyroid imaging," Neuroimaging Clin N Am 18(3), 537-549, ix (2008)

22. A. Mahadevan-Jansen and R. Richards-Kortum, "Raman Spectroscopy for the detection of cancers and precancers," J Biomed Opt 1(1), 31-70 (1996)

23. E. B. Hanlon, R. Manoharan, T. W. Koo, K. E. Shafer, J. T. Motz, M. Fitzmaurice, J. R. Kramer, I. Itzkan, R. R. Dasari and M. S. Feld, "Prospects for in vivo Raman spectroscopy," Physics in medicine and biology 45(2), R1-R59 (2000)

24. R. J. Colthrup, L. H. Daly, S. E. Wiberley Infrared and Raman spectroscopy, Academic Press (3rd Edition), (1991).

25. M. V. P. Chowdary, K. K. Kumar, J. Kurien, S. Mathew and C. M. Krishna, "Discrimination of normal, benign, and malignant breast tissues by Raman spectroscopy," Biopolymers 83(5), 556-569 (2006)

26. T. R. Hata, T. A. Scholz, I. V. Ermakov, R. W. McClane, F. Khachik, W. Gellermann and L. K. Pershing, "Non-invasive Raman spectroscopic detection of carotenoids in human skin," Journal of Investigative Dermatology 115(3), 441-448 (2000)

27. M. G. Shim, L. Song, N. E. Marcon and B. C. Wilson, "In vivo near-infrared Raman spectroscopy: Demonstration of feasibility during clinical gastrointestinal endoscopy," Photochemistry and Photobiology 72(1), 146-150 (2000)

28. A. P. Oliveira, R. A. Bitar, L. Silveira, R. A. Zangaro and A. A. Martin, "Near-infrared Raman spectroscopy for oral carcinoma diagnosis," Photomedicine and Laser Surgery 24(3), 348-353 (2006)

29. A. Mahadevan-Jansen, W. F. Mitchell, N. Ramanujam, U. Utzinger and R. Richards-Kortum, "Development of a fiber optic probe to measure NIR Raman spectra of cervical tissue in vivo," Photochemistry and Photobiology 68(3), 427-431 (1998)

30. C. Arens, K. Malzahn, O. Dias, M. Andrea and H. Glanz, "[Endoscopic imaging techniques in the diagnosis of laryngeal carcinoma and its precursor lesions]," Laryngo- rhino- otologie 78(12), 685-691 (1999)

31. G. Giubileo, F. Colao, A. Puiu, G. Panzironi, F. Brizzi and P. Rocchini, "Fluorescence spectroscopy of normal and follicular cancer samples from human thyroid," Spectroscopy 19(2), 79-87 (2005)

32. G. Liu, J. H. Liu, L. Zhang, F. Yu and S. Z. Sun, "Raman spectroscopic study of human tissues," Guang Pu Xue Yu Guang Pu Fen Xi (Chinese Journal – Translated to English), 25(5), 723-725 (2005)

33. C. Medina-Gutierrez, J. L. Quintanar, C. Frausto-Reyes and R. Sato-Berru, "The application of NIR Raman spectroscopy in the assessment of serum thyroid-stimulating hormone in rats," Spectrochim Acta A Mol Biomol Spectrosc 61(1-2), 87-91 (2005)

34. M. J. Pitman, J. M. Rosenthal, H. E. Savage, G. Yu, S. A. McCormick, A. Katz, R. R. Alfano and S. P. Schantz, "The fluorescence of thyroid tissue," Otolaryngol Head Neck Surg 131(5), 623-627 (2004)

35. R. L. Prosst, F. Willeke, L. Schroeter, S. Post and J. Gahlen, "Fluorescence-guided minimally invasive parathyroidectomy: a novel detection technique for parathyroid glands," Surg Endosc 20(9), 1488-1492 (2006)

36. Z.V. Jaliashvili, T.D. Medoidze, K.M. Mardaleishvili, J.J. Ramsden, Z.G. Melikishvili "Laser induced fluorescence model of human goiter," Laser Meth Chem Biol Med, 5(3) pp. 217-219 (2008).

37. N. Ramanujam, M. F. Mitchell, A. Mahadevan-Jansen, S. L. Thomsen, G. Staerkel, A. Malpica, T. Wright, N. Atkinson and R. Richards-Kortum, "Cervical precancer detection using a multivariate statistical algorithm based on laser-induced fluorescence spectra at multiple excitation wavelengths," Photochem Photobiol, 64(4), 720-735 (1996)

38. N. Ramanujam, "Fluorescence spectroscopy of neoplastic and non-neoplastic tissues," Neoplasia 2(1-2), 89-117 (2000)

39. J. R. Lakowicz, "Introduction to Fluorescence," in Principles of Fluorescence Spectroscopy, pp. 1-26, Springer (3rd Edition), (2006).

40. J. R. Lakowicz, "Fluorophores," in Principles of Fluorescence Spectroscopy, pp. 63-95, Springer, (3rd Edition), (2006).

41. S. G. Demos, R. Bold, R. D. White and R. Ramsamooj, "Investigation of near-infrared autofluorescence imaging for the detection of breast cancer," Ieee J Sel Top Quant 11(4), 791-798 (2005)

42. X. Han, H. Lui, D. I. McLean and H. S. Zeng, "Near-infrared autofluorescence imaging of cutaneous melanins and human skin in vivo," Journal of Biomedical Optics 14(2), - (2009)

43. G. Doherty, "Thyroid and Parathyorid," in Oncology: an evidence-based approach (A. E. Chang, P. A. Ganz, D. F. Hayes, T. Kinsella, H. I. Pass, J. H. Schiller, R. M. Stone, V. Strecher – Editors), Springer, (1st Edition) (2006).

44. A. Mahadevan-Jansen, M. F. Mitchell, N. Ramanujam, U. Utzinger and R. Richards-Kortum, "Development of a fiber optic probe to measure NIR Raman spectra of cervical tissue in vivo," Photochemistry and photobiology 68(3), 427-431 (1998)

45. C. Paras, Keller M, White L, Whisenant J, Gasparino N, Phay J, Mahadevan-Jansen A, "Optical guidance of endocrine surgery (7169-59)," in SPIE Photonics West Bios, unplished conference proceedings SPIE, San Jose, CA (2009).

46. E. Tanaka, H. S. Choi, H. Fujii, M. G. Bawendi and J. V. Frangioni, "Image-guided oncologic surgery using invisible light: completed pre-clinical development for sentinel lymph node mapping," Ann Surg Oncol 13(12), 1671-1681 (2006)

47. J. V. Frangioni, "In vivo near-infrared fluorescence imaging," Curr Opin Chem Biol 7(5), 626-634 (2003)

48. S. G. Demos, R. Bold, R. V. White and R. Ramsamooj, "Investigation of near-infrared autofluorescence imaging for the detection of breast cancer," Selected Topics in Quantum Electronics, IEEE Journal of 11(4), 791-798 (2005)

49. X. Han, H. Lui, D. I. McLean and H. Zeng, "Near-infrared autofluorescence imaging of cutaneous melanins and human skin in vivo," J Biomed Opt 14(2), 024017 (2009)

50. C. N. Keilhauer and F. C. Delori, "Near-infrared autofluorescence imaging of the fundus: visualization of ocular melanin," Invest Ophthalmol Vis Sci 47(8), 3556-3564 (2006)

51. X. Shao, W. Zheng and Z. Huang, "Near-infrared autofluorescence imaging for colonic cancer detection," in Optical Sensors and Biophotonics, pp. 76340B-76345, SPIE, Shanghai, China (2009).

52. K. Das, N. Stone, C. Kendall, C. Fowler and J. Christie-Brown, "Raman spectroscopy of parathyroid tissue pathology," Lasers Med Sci 21(4), 192-197 (2006)

53. L. Sherwood, "Human physiology: from cells to systems" Brooks Cole; (7^{th} Edition) (2009).

54. G. Doherty, "Thyroid and Parathyorid," in Oncology: an evidence-based approach (A. E. Chang, P. A. Ganz, D. F. Hayes, T. Kinsella, H. I. Pass, J. H. Schiller, R. M. Stone, V. Strecher – Editors), Springer, (1^{st} Edition) (2006).

55. J. K. Harness, J. A. van Heerden, S. Lennquist, M. Rothmund, B. H. Barraclough, A. W. Goode, I. B. Rosen, Y. Fujimoto and C. Proye, "Future of thyroid surgery and training surgeons to meet the expectations of 2000 and beyond," World J Surg 24(8), 976-982 (2000)

56. S. Ozbas, S. Kocak, S. Aydintug, A. Cakmak, M. A. Demirkiran and G. C. Wishart, "Comparison of the complications of subtotal, near total and total thyroidectomy in the surgical management of multinodular goitre," Endocrine journal 52(2), 199-205 (2005)

57. T. Reeve and N. W. Thompson, "Complications of thyroid surgery: how to avoid them, how to manage them, and observations on their possible effect on the whole patient," World J Surg 24(8), 971-975 (2000)

58. C. Paras, M. Keller, L. White, J. Phay and A. Mahadevan-Jansen, "Near-infrared autofluorescence for the detection of parathyroid glands," J Biomed Opt 16(6), 067012 (2011)

59. J. R. Lakowicz, Principles of fluorescence spectroscopy, Springer, (3rd Edition), (2006).

60. Z. Huang, H. Lui, X. K. Chen, A. Alajlan, D. I. McLean and H. Zeng, "Raman spectroscopy of in vivo cutaneous melanin," J Biomed Opt 9(6), 1198-1205 (2004)

61. E. Berber, R. T. Parikh, N. Ballem, C. N. Garner, M. Milas and A. E. Siperstein, "Factors contributing to negative parathyroid localization: an analysis of 1000 patients," Surgery 144(1), 74-79 (2008)

62. D. L. Fraker, H. Harsono and R. Lewis, "Minimally invasive parathyroidectomy: benefits and requirements of localization, diagnosis, and intraoperative PTH monitoring. long-term results," World J Surg 33(11), 2256-2265 (2009)

63. O. Hessman, P. Stalberg, A. Sundin, U. Garske, C. Rudberg, L. G. Eriksson, P. Hellman and G. Akerstrom, "High success rate of parathyroid reoperation may be achieved with improved localization diagnosis," World J Surg 32(5), 774-781; discussion 782-773 (2008)

64. A. Komisar, "Parathyroid localization," Operative Techniques in Otolaryngology-Head and Neck Surgery 13(3), 219-222 (2002)

65. J. I. Lew and C. C. Solorzano, "Surgical management of primary hyperparathyroidism: state of the art," Surg Clin North Am 89(5), 1205-1225 (2009)

66. R. Prommegger, G. Wimmer, C. Profanter, T. Sauper, M. Sieb, P. Kovacs, R. Bale, D. Putzer, M. Gabriel and R. Margreiter, "Virtual neck exploration: a new method for localizing abnormal parathyroid glands," Ann Surg 250(5), 761-765 (2009)

67. S. B. Reeder, T. S. Desser, R. J. Weigel and R. B. Jeffrey, "Sonography in primary hyperparathyroidism: review with emphasis on scanning technique," Journal of ultrasound in medicine : official journal of the American Institute of Ultrasound in Medicine 21(5), 539-552; quiz 553-534 (2002)

68. M. E. Spieth, J. Gough and D. L. Kasner, "Role of US with supplemental CT for localization of parathyroid adenomas," Radiology 223(3), 878-879; author reply 879 (2002)

69. M. E. Tublin, D. A. Pryma, J. H. Yim, J. B. Ogilvie, J. M. Mountz, B. Bencherif and S. E. Carty, "Localization of parathyroid adenomas by sonography and technetium tc 99m sestamibi single-photon emission computed tomography before minimally invasive parathyroidectomy: are both studies really needed?," J Ultrasound Med, 28(2), 183-190 (2009)

70. L. Knudsen, C. K. Johansson, P. A. Philipsen, M. Gniadecka and H. C. Wulf, "Natural variations and reproducibility of in vivo near-infrared Fourier transform Raman spectroscopy of normal human skin," J Raman Spectrosc 33(7), 574-579 (2002)

71. E. Vargis, T. Byrd, Q. Logan, D. Khabele and A. Mahadevan-Jansen, "Sensitivity of Raman spectroscopy to normal patient variability," J Biomed Opt 16(11), 117004 (2011)

72. S. A. Prahl, M. J. van Gemert and A. J. Welch, "Determining the optical properties of turbid mediaby using the adding-doubling method," Appl Opt 32(4), 559-568 (1993)

73. N. Chattopadhyay and E. M. Brown, "Cellular "sensing" of extracellular calcium (Ca(2+)(o)): emerging roles in regulating diverse physiological functions," Cellular signalling 12(6), 361-366 (2000)

74. E. M. Brown, G. Gamba, D. Riccardi, M. Lombardi, R. Butters, O. Kifor, A. Sun, M. A. Hediger, J. Lytton and S. C. Hebert, "Cloning and characterization of an extracellular Ca(2+)-sensing receptor from bovine parathyroid," Nature 366(6455), 575-580 (1993)

75. L. D'Souza-Li, "The calcium-sensing receptor and related diseases," Arquivos brasileiros de endocrinologia e metabologia 50(4), 628-639 (2006)

76. D. Goltzman, "Hormone Secretion," in Principles and practice of endocrinology and metabolism (K. L. Becker – Editor), pp. xxxiv, 2477 p., Lippincott Williams and Wilkins, (2001).

77. E. M. Brown, "Hormonal Control of Calcium Homeostasis," in Principles and Practice of Endocrinology & Metabolism (K. L. Becker - Editor), p. 482, Lippincott Williams & Wilkins, (2001).

78. O. Kifor, F. D. Moore, Jr., P. Wang, M. Goldstein, P. Vassilev, I. Kifor, S. C. Hebert and E. M. Brown, "Reduced immunostaining for the extracellular Ca2+-sensing receptor in primary and uremic secondary hyperparathyroidism," J Clin Endocrinol Metab 81(4), 1598-1606 (1996)

79. A. Kienle and T. Glanzmann, "In vivo determination of the optical properties of muscle with time-resolved reflectance using a layered model," Phys Med Biol 44(11), 2689-2702 (1999)

80. S. R. Anderson, A. Vaughn, D. Karakla and J. T. Wadsworth, "Effectiveness of surgeon interpretation of technetium tc 99m sestamibi scans in localizing parathyroid adenomas," Arch Otolaryngol Head Neck Surg 134(9), 953-957 (2008)

81. N. Ramanujam, M. F. Mitchell, A. Mahadevan, S. Thomsen, A. Malpica, T. Wright, N. Atkinson and R. Richards-Kortum, "Spectroscopic diagnosis of cervical intraepithelial neoplasia (CIN) in vivo using laser-induced fluorescence spectra at multiple excitation wavelengths," Lasers Surg Med 19(1), 63-74 (1996)

82. FJW Optical Systems, http://www.findrscope.com/ (2012).

83. K. Zanocco, P. Angelos and C. Sturgeon, "Cost-effectiveness analysis of parathyroidectomy for asymptomatic primary hyperparathyroidism," Surgery 140(6), 874-881; discussion 881-872 (2006).